EFFECT OF PORE SIZE AND THICKNESS ON CRITICAL PRESSURE OF ELASTIC SYSTEMS

A Thesis
Presented to
The Academic Faculty

By

Barton P Carter

In Partial Fulfillment
Of the Requirements for the Degree
Master of Science in Mechanical Engineering

Georgia Institute of Technology

August 2005

EFFECT OF PORE SIZE AND THICKNESS ON CRITICAL PRESSURE OF ELASTIC SYSTEMS

Approved by:

Dr. David I. Orloff, Advisor
School of Mechanical Engineering
Georgia Institute of Technology

Dr. Timothy Patterson
School of Mechanical Engineering
Georgia Institute of Technology

Dr. Frederick W. Ahrens
School of Mechanical Engineering
Georgia Institute of Technology

Date Approved: July 15, 2005

ACKNOWLEDGEMENTS

I would like to extend a heart-felt and sincere thank you to Dr. David Orloff; working with him has been the highlight of my academic career. His support and guidance throughout this project have been invaluable. He has taught me how fulfilling research can be; even it does sometimes test one's will.

I would like to thank Dr. Tim Patterson and Dr. Fred Ahrens for serving on my committee and for the input they have given to this project. I am also very grateful to Dr. Fred Bloom for his assistance and insights into the thorny mathematics of membranes. I would also like to thank Chris Humphries and Matt Moore for their assistance and dedication in the lab. I would like to express appreciation to Mark Urbin, Perry Arrington, as well as the staff of GTRI Machine services for their assistance in construction of all the materials necessary for this project.

TABLE OF CONTENTS

Acknowledgements iii

List of Tables vi

List of Figures vii

List of Symbols ix

Summary x

Chapter 1 Introduction 1

Background 1

Previous Work 1

Current Work 3

Chapter 2 Literature Review 5

Chapter 3 Math Model 10

Membrane Deflection 12

Critical Tension 13

Simple Griffith Criterion 14

Griffith Criterion with Radial Strain 16

Chapter 4 Methodology 19

Elastic Properties of Latex 19

Critical Tension & Critical Energy Release Rate 21

Critical Pressure 26

Perforation Test 31

Chapter 5 Results and Discussion 34

Thickness Gradient 34

Elastic Behavior 35
Poisson Ratio 37
Peel Test 37
Critical Pressure 38
Perforation Test 39
Chapter 6 Conclusion and Recommendations for Future Work 44
APPENDIX A Raw Data 48
A.1 Peel Tests 49
A.2 Critical Pressure Results 50
A.3 Perforation Tests 51
A.4 Iterative Solutions to Griffith Polynomial 53
APPENDIX B Sample Calculations 54
B.1 Critical Tension Sample Calculations 55
B.2 Simple Griffith Model Sample Calculations 56
B.3 Griffith Model with Radial Strain Sample Calculations 57
APPENDIX C Image Analysis 58
C.1 Image Analysis 59
APPENDIX D Math Model 64
D.1 Math Model 65

LIST OF TABLES

Table 3-1: Failure Criteria for Delamination 18

Table 5-1: Peel Test Results 38

Table A-1: Results from Peel Tests of Latex and Epoxy 49

Table A-2: Pressure Experiment Results 50

Table A-3: Raw Data for Black Tape Perforation Tests 51

Table A-4: Average Values for Black Tape 51

Table A-5: Raw Data for Clear Tape Perforation Tests 52

Table A-6: Average Values for Clear Tape 52

Table A-7: Solutions from EES for λ_c as a function of Defect Radius 53

LIST OF FIGURES

Figure 1.1: Conceptual View of Delamination Parameters 3

Figure 2.1: Schematic of Adhesive and Cohesive Failure 7

Figure 2.2: Schematic of Peel Experiment 9

Figure 3.1: Schematic of Deflection of an Elastic Membrane 11

Figure 3.2: Schematic of Tension Component 13

Figure 4.1: Instron 1122 used for Tensile Tests 20

Figure 4.2: Peel Test Schematic 23

Figure 4.3: Schematic of Peel Test Output 24

Figure 4.4: Stainless Steel Substrate 24

Figure 4.5: Peel Test 25

Figure 4.6: Critical Pressure Experiment Schematic 27

Figure 4.7: Critical Pressure Apparatus 27

Figure 4.8: Fluid Reservoir 28

Figure 4.9: Critical Pressure Plates 29

Figure 4.10: Pretensioned Elastic Membrane 30

Figure 4.11: Elastic Membrane Delaminating 31

Figure 5.1: Variation of Thickness for Latex Sheets 34

Figure 5.2: Variation of width throughout latex sheets 35

Figure 5.3: Overall Elastic Behavior of Latex Sheets 35

Figure 5.4: Linear Tensile Range for Peel Tests 36

Figure 5.5: Linear Tensile Range for Tensioning Elastic Membranes 37

Figure 5.6: Peel Test Example 38

Figure 5.7: Comparison Experimental and Theoretical Critical Pressures 39

Figure 5.8:Results of Perforation on Delamination of Black Tape 40

Figure 5.9: Results of Perforation on Delamination of Clear Tape 41

Figure 5.10: Results of Perforation Test Including Geometric Effect for Black Tape 42

Figure 5.11: Results of Perforation Test Including Geometric Effect for Clear Tape 43

Figure 6.1: Schematic of Z-Toughness Apparatus for Wet Paper 46

Figure 6.2: Z-Toughness Jaws for Future Work 46

Figure C.1: Original Picture with Scale 60

Figure C.2: Set the Scale 61

Figure C.3: Adjust Threshold 62

Figure C.4: Measure the Defect Area 63

LIST OF SYMBOLS (IN ORDER OF APPEARANCE)

a – defect radius

G_a – critical energy release rate

F – Load to peel membrane

G – energy release rate

U_{ext} – external work

U_s – strain energy

U_d – dissipated energy

U_k – kinetic energy

b – specimen width

θ – angle of peel

ε – strain

h – specimen thickness

λ - pressure

w – vertical deflection

τ – tension

w_m – maximum vertical deflection

r – defect radius

τ^c – critical tension

τ_z – vertical component of tension

ϕ – angle of deflection

λ_c – critical pressure

ρ – density

Π_a – total energy

A - area

R_a – domain of integration

K – bending stiffness

Φ - Airy's Stress Function

w_o – initial defect deflection

E – Young's Modulus

ν – Poisson's Ratio

U_a – Net Strain Energy

u_r – radial displacement

V_a – potential energy

σ - stress

A_c – cross-sectional area

F_c – critical force

λ_{defect} – experimental pressure at the defect

γ - specific weight of fluid

z_m –height of manometer fluid head

z_f - height of fluid reservoir fluid head

ε' - lateral strain

A_s – surface area

SUMMARY

Significant energy savings can be achieved by improving efficiency of water removal in the press section of a paper machine, rather than energy-intensive evaporative dryer cans. Impulse drying is a novel technology to remove water from the sheet in the press section by using a heated press roll.

Delamination is a major challenge to be overcome before impulse drying can be implemented successfully. Delamination is caused by a region of high temperature liquid water under high pressure in the press. Upon exiting the nip, the pressure drops and the high temperature water flashes to steam. If the expansion of the steam is too strong, the bonds between the fibers will fail and a blister will form. The formation of this blister is characteristic of delamination.

The goal of this project was to understand the internal mechanics of a wet web as it exits the nip of an impulse dryer. In this way, the components of the sheet can be tailored to open the operating window of impulse drying. A mathematical model, developed to describe the deflection and delamination of an elastic membrane, was utilized in this work. Three failure criteria were employed to represent delamination of this pliable membrane from the more rigid sub layers in the sheet.

The experimental portion of this effort was devoted to showing the validity of these models and which was the best fit. A series of experiments were employed to validate the model. A peel test was used to determine the amount of work needed to pull a membrane from a rigid substrate. Pressurized blister experiments were conducted to find the relationship between critical pressure and initial defect size. The predictions

from the mathematical model were then compared to these experimental values. Finally, work was done to understand the physics of the delamination of a porous membrane.

Chapter 1 Introduction

Background

Energy consumption in paper production is a key concern. Removal of water from the web using evaporative dryer cans is highly energy intensive. Cost of energy utilization can be reduced significantly by using impulse dryers. There is about a 15:1 energy consumption ratio between the dryer and press section of a paper machine [1]. It has been shown that a one percent gain in solids produces a four percent energy savings in the dryer section [1]. Considering 75% of the energy consumed in the typical paper machine is used in the dryer section [2]; a small gain in solids content in the press section leads to significant overall energy savings.

Delamination of impulse dried sheets is a major obstacle to implementing the technology. Delamination is caused by a region of high temperature liquid water under high pressure in the press. Upon exiting the nip the pressure drops and the high temperature water flashes to steam. If the expansion of the steam is too strong, the bonds between the fibers will fail and a blister will form. The formation of this blister is indicative of delamination. The purpose of this thesis is to understand the fundamentals that influence blistering.

Previous Work

A substantial body of work has been devoted to understanding what causes delamination and how it might be alleviated.

Work was carried out using variable nip exit pressures. The hypothesis that delamination is caused by an imbalance of internal and external sheet pressure was tested

by Krause [3] and Parviainen [4]. The purpose of this study was to measure the temperature profile of impulse dried sheets both at elevated and ambient exit pressures. The work for this study was conducted in two parts. First, the elevated ambient exit pressure necessary to initiate delamination was found, these elevated ambient pressures are known as critical ambient pressures. Second, temperature profiles were determined by placing thermocouples in layered sheets as they were impulse dried in an MTS press. It was found that there was a maximum pressure difference between the internal and external pressure delamination begins.

Figure 1.1, shows a conceptual view of temperature, moisture, and pressure profiles in a sheet during impulse drying. The top surface is in contact with the heated press roll, and the bottom with the unheated felt. Temperature and pressure are highest at the press interface and drop to their minimums at the felt interface; the moisture on the other hand increases from its minimum to its maximum between the press and felt. There are three distinct regions of the sheet. In region A, there is little water in the pores, and it is at a high temperature. In region B, the pores contain liquid water and are at a moderately high temperature. In region C, the pores have a high moisture value and are at a low temperature. Region B of the sheet contains enough water and has a sufficiently high temperature to produce steam at atmospheric pressure. Thus as the sheet exits the nip, and the pressure suddenly drops to atmospheric pressure the liquid water in region B, flashes to steam. If the fiber network is not strong enough to contain the expansion, delamination will occur.

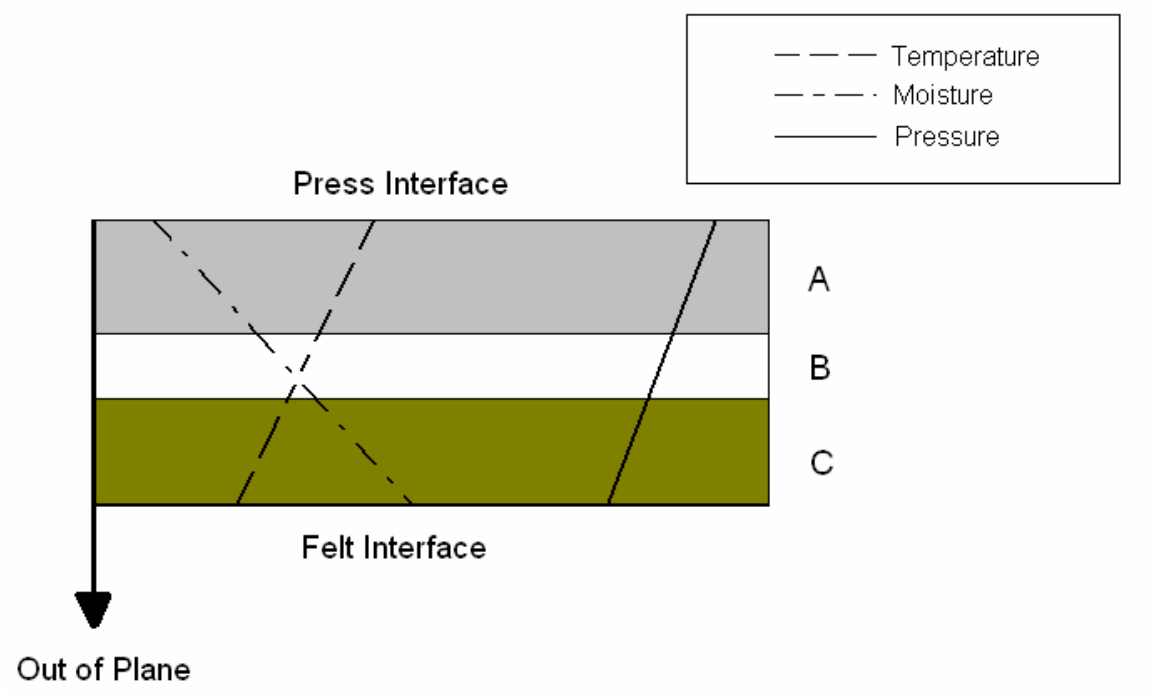

Figure 1.1: Conceptual View of Delamination Parameters

Additional work was done by Boerner [5]; a low thermal mass ceramic coating was applied to the press section of a pilot paper machine. This ceramic surface decreased the quantity of heat conducted to the sheet during pressing in comparison with typical hot pressing; this resulted in lower post press temperatures. Lower temperatures within the sheet inhibit the likelihood of delamination. It was shown that a 400 g/m^2 sheet with a freeness as low as 600 CSF could be impulse dried without initiating delamination in the fiber network. Critical temperatures were also found for these sheets at different freeness. Critical temperature is the heated press temperature at which delamination begins to occur. Based on these results it was postulated that higher freeness sheets allow for steam venting through the heated side of the sheet thus elevating delamination.

Current Work

Previous work in this area considers largely external factors (e.g. Critical Platen Temperature, Critical Ambient Pressure). This project has centered on what factors in

the structure of the wet web are important. It should then be possible to characterize what variables in the furnish could be modified to inhibit delamination.

Linear elastic fracture mechanics (LEFM) was used to characterize delamination. A mathematical model [6], was developed to describe the deflection and delamination of an elastic membrane. The model develops three failure criteria to characterize sheet delamination. While differing in some ways, each of these criteria indicate that the critical pressure of delamination is inversely proportional to the initial defect radius.

The goal of this investigation was to validate the math model. Three sets of experiments were necessary to validate the model. Tensile tests were performed to understand the elastic properties of the membrane that was used. Peel tests were used to find the critical tension and energy release rate for the elastic-adhesive system. Finally, a set of pressurized blister tests were conducted with elastic membranes adhered to a rigid substrate. The critical pressure of delamination was experimentally found to be inversely proportional to the radius of the initial defect (analogous to a pore radius in a wet paper web).

It is important to recognize that pores within a wet web are not closed systems. Hence, an additional set of blister tests were performed with a perforation in the elastic membrane to simulate venting. The perforations were found to increase the critical pressure, as anticipated..

Chapter 2 Literature Review

The problem of quantifying adhesive strength is not a new one. There are a number of difficulties associated with the problem. Key among them is how to approach the problem. Is it the energy need to decrease the sum of the surface energies, or the work needed to break the bonds?

In 1961, Dannenberg [7] proposed the pressurized blister test, a method for measuring adhesion of organic coating to metals and other substrates. Dannenberg [7] discussed a number of techniques both qualitative and quantitative; these ranged from the use of a sharp knife in an experienced hand to a centrifuge that measures the force of failure. All of these prior methods had limitations. The method outlined by Dannenberg [7] would (1) measure adhesion instead of cohesion, (2) have the capability of being applied to a wide variety of specimens, and (3) give precise results expressed in physical units.

The concept was to inject a fluid between a substrate and coating in such a way that the adhesive fails in the form of a blister. Dannenberg [7] used aluminum foil adhered to a slotted plate with a weak rubber cement. An oblong blister was used because it was found to be more stable with more reproducible results. Mercury was the working fluid; it was pumped into the plate at a steady rate. The pressure was also measured and recorded as a function of time. The work done by the fluid was found by integrating the pressure and volume of the fluid.

The value of Dannenberg's [7] work was that it gave a method for quantifying adhesives. In subsequent yeats, pressurized blister tests have been used for paints, microelectronics and a plethora of other adhesive applications.

While Dannenberg [7] is often credited as the progenitor of the pressurized blister test, Williams is responsible for the blister test in its current form. Williams reviewed the work of Griffith regarding the use of an overall energy balance to equate the reduction in strain energy to the energy required to create a new surface. Williams then compared the approaches for both a continuum and dissimilar media.

Williams [8] interpreted the difference between adhesive and cohesive failure as a difference between the surfaces created. The amount of incremental energy per unit thickness released for cohesive failure was twice that of adhesive failure because in the case of cohesion two new surfaces were created. This view is consistent with Dannenberg [7], who made the observation that cohesive energy release rate was fracture in the adhesive itself; while adhesive energy release rate is acceptable when a crack would propagates at the interface of adhesive and the adherand. A conceptual view of this is shown in Figure 2.1. For the work of this study the adhesive energy release rate was employed. Future work, involving wet paper, would most likely need to consider the cohesive energy release rate of the wet web.

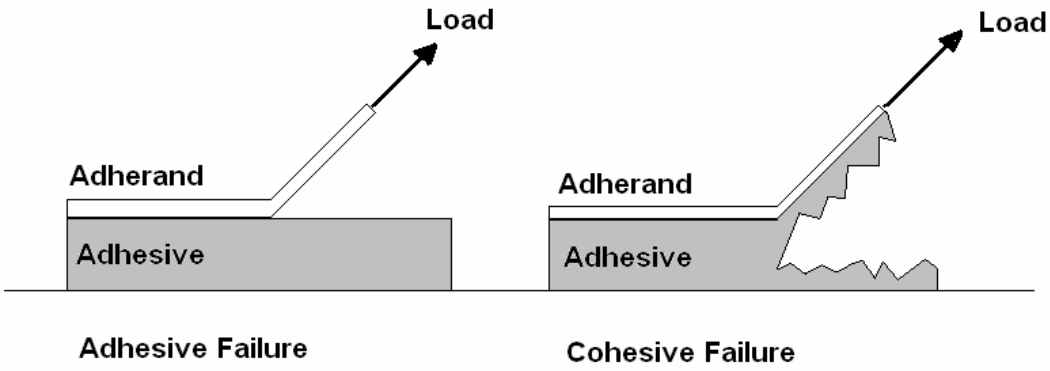

Figure 2.1: Schematic of Adhesive and Cohesive Failure

Williams then compared solutions of fracture problems under hydrostatic pressure for both thick and thin membrane specimens. Using these, he provided a method to estimate the adhesive energy.

Gent & Lewandowski [9]conducted work on the pressurized blister test for widely varying thicknesses, they developed an understanding of the transition cases in Williams' previous work. They considered three cases: (1) when the blister diameter was much smaller than the thickness of the adhering layer, (2) when the blister diameter was comparable to the thickness of the adhering layer, (3) when the blister diameter was much larger than the thickness of the adhering layer. The critical pressures (blow off pressures) for the first two cases were proportional to the initial defect radius to the (-½) power; consistent with plate theory. While in the third case, the critical pressure was inversely proportional to the initial defect radius. It is worth noting that the first and third case are the limiting cases discussed by Williams and the second is the more difficult transition case between plate and membrane behavior. Gent and Lewandowski's experimental work was with tape as the adhering layers. Specifically, two types of tape

were employed with different thicknesses; they had similar strengths of adhesion, but very different tensile properties.

The critical energy release rate was found by employing a simple inextensible peel test, where G_a=F/w; F was the peel load, and w was the width of the specimen. Delamination experiments were then conducted at varying initial defect diameters and varying thicknesses with a constant rate of volumetric increase. From these delamination tests, Gent and Lewandowski found the exact value for G_a by establishing the total work done on the system. They found the actual critical energy release rate was always less than that found from the peel test. They also found an inverse relationship between the critical pressure and blister diameter for the third case.

Williams [10] derived several solutions for the energy release rates. Peel tests are a common test to evaluate adhesion and critical energy release rates. Williams defined the energy release rate of a peeling flexible membrane as:

$$G = \frac{d}{dA}\left[U_{ext} - U_s - U_d - U_k\right] \tag{2.1}$$

Where U_{ext} is the external work done on the specimen, U_s is the strain energy, U_k is kinetic energy, U_d is dissipated energy, and A is the area created. For most experiments slow peeling is recommended for evaluating elastic membranes. If one integrates the strain energy, the energy release rate becomes:

$$G = \frac{F}{b}\left(1 - \cos\theta + \frac{\varepsilon}{2}\right) \tag{2.2}$$

A schematic of this experiment is shown in Figure 2.2. This represents one of the simplest experimental methods for determining the critical energy release rate.

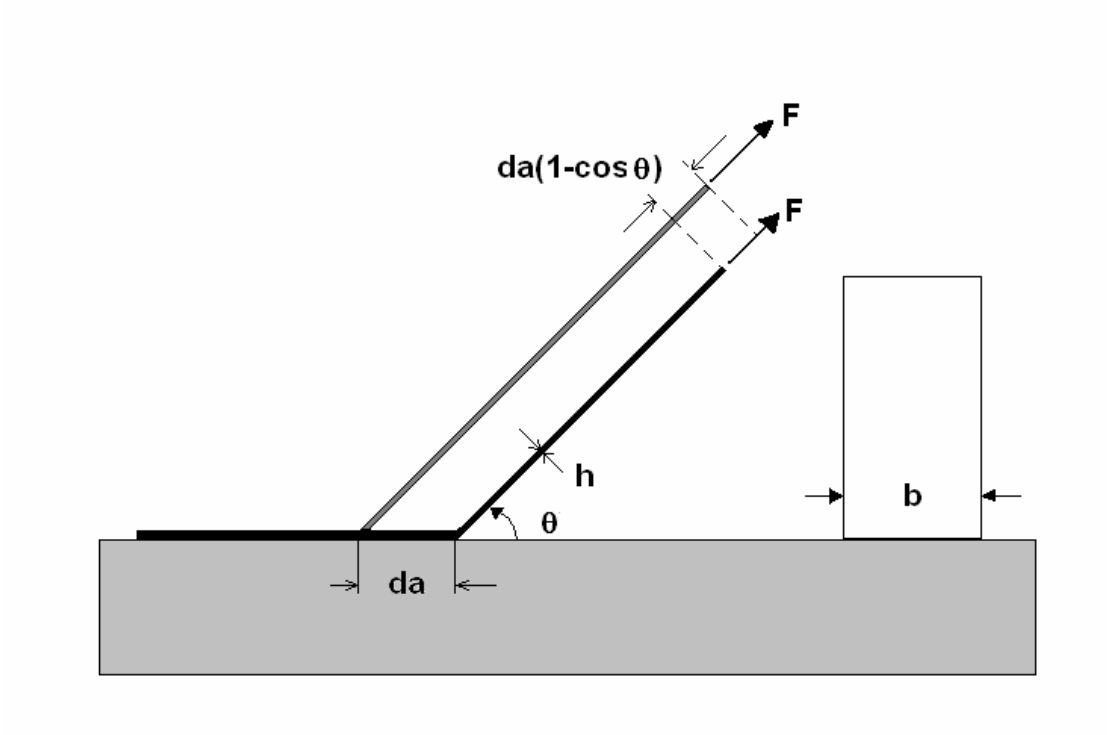

Figure 2.2: Schematic of Peel Experiment

Williams [10] then derived a number of solutions of energy release rates for a variety of geometries (i.e. debonded strips, blisters, axisymmetric membranes, etc) under various loading conditions (i.e. concentrated load, uniform pressure). His work questions some earlier work. For example, Williams suggests that, Hinkley's [11] values are incorrect because of an incorrect energy balance. It is noted that Williams' [10] values are in close agreement with Gent & Lewandowski [9], which give the exact result. Williams [10] concludes by saying the differences between the exact results and peel tests are small for uniform pressure loading, while the differences for concentrated loads are significant.

Chapter 3 Math Model

The mathematical model [6] which describes the delamination of the elastic layer was a central part of this project; the model was developed by Dr. Fred Bloom for the purpose of this project. The model consists of three criteria which characterize the failure of the bonds adhering the elastic membrane to the rigid substrate. The details of the model are given in Appendix D.

The portion of the model discussing deflection is based on the assumption that there is an isotropic elastic material with a well defined initial defect within the wet web. For the case of delamination of a wet web this debonded area, a pore is pressurized uniformly by an internal pressure λ. This represents the pressure of steam expansion within the sheet as it exits the nip. This pressure causes the wet paper, modeled as an elastic membrane to deflect. A schematic of this is shown in Figure 3.1. The membrane deflection increases with increase in pressure, until it reaches a critical pressure and the adhesive is no longer able to hold the adhered membrane. The specifics of these failure criteria are discussed in detail in this chapter.

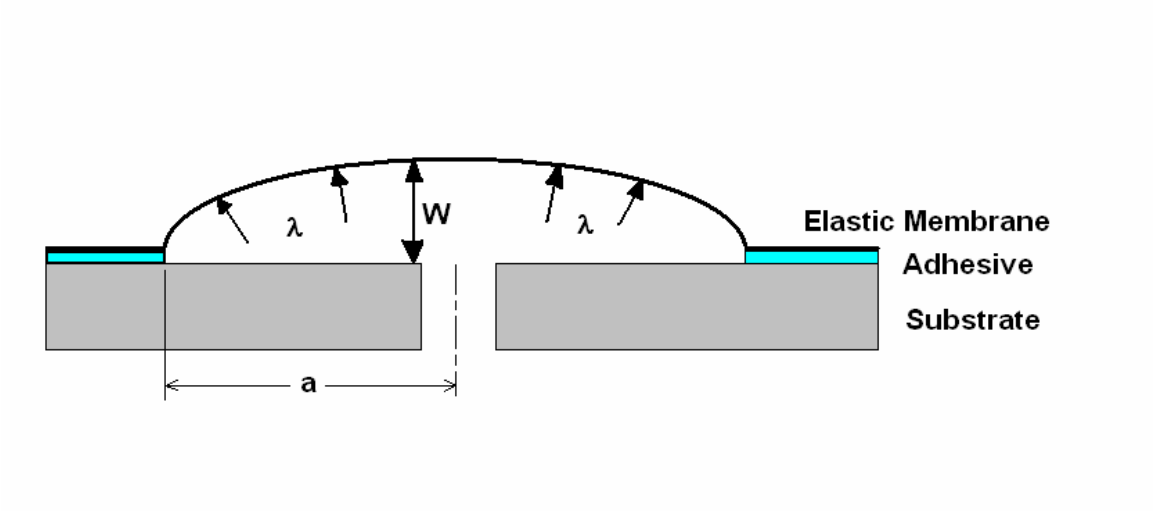

Figure 3.1: Schematic of Deflection of an Elastic Membrane

There are two major assumptions (1) the wet web is an isotropic continuum, (2) paper acts in an elastic fashion upon exiting the nip of an impulse dryer. Obviously paper is not a continuum; it is made up of fibers, lignin, water, and various chemical compounds. However, paper does exhibit bulk behavior in the same manner as many other materials. Many materials such as iron, copper, plastics, etc are assumed to be continuous materials, even though they are composed of masses of crystals and voids or polymer chains. To have a closed form solution to the problem of internal strength and adhesion it is necessary to assume the material is one whose composition does not vary throughout its thickness. Therefore, assuming that this particular layer (Region B) in paper is a continuum with a debonded pore region is altogether reasonable.

Paper is not typically what one would describe as an elastic material either. Paper even in its dry form is generally considered viscoelastic. However, ror very short time periods time dependent effects can be neglected leaving only the elastic response. The dwell time in the press is approximately 20 to 40 ms, and the expansion of the steam is on

an even shorter time-scale. Under these circumstances, an elastic model for paper is well justified.

Membrane Deflection

These models utilize a two dimensional wave equation, also known as a membrane equation, to describe deflection of the adhering membrane. Membrane equations are a simplification of plate equation where the bending stiffness is negligible. The membrane equation is dependent on the fact that there is some amount of pre-tension in the sheet; this tension is represented by τ.

$$W_{,rr} + \frac{1}{r} W_{,r} = \frac{-\lambda}{\tau} \tag{3.1}$$

Where W is the vertical deflection, λ is the pressure, and r is the radial distance from the center of the defect. It follows that if λ is a uniform pressure throughout the defect that deflection profile for an axisymmetric blister is:

$$W - W_m = \alpha \cdot r^2 \tag{3.2}$$

and W(a)=0 it follows that $\alpha = \frac{W_m}{a^2}$, where W_m is the maximum deflection,

$$W(r) = W_m \left(1 - \left(\frac{r}{a} \right)^2 \right) \tag{3.3}$$

This can be further reduced to an equation that depends only on the geometry, applied pressure, and magnitude of tension in the sheet.

$$W(r) = \frac{\lambda}{4\tau} \left(a^2 - r^2 \right) \tag{3.4}$$

Critical Tension

The first model is simple in its approach. It holds that there is a certain critical tension (force per unit length) denoted by τ^c of the glue bond perpendicular to the surface of the substrate at which the glue bond will fail. This τ^c is the out of plane component of the magnitude of the tension in the sheet. This is shown in Figure 3.2.

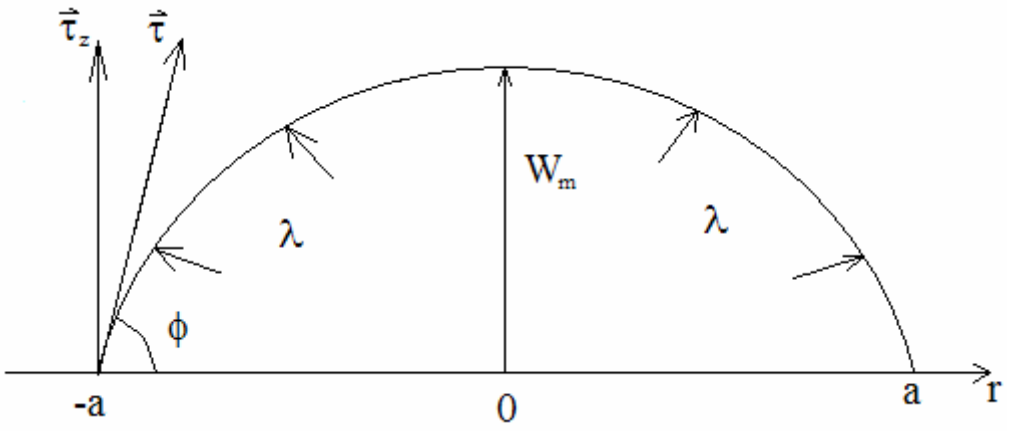

Figure 3.2: Schematic of Tension Component

It follows that the component of τ, τ^c is

$$\tau_z = \tau \sin\phi \tag{3.5}$$

Note from (3.3) that

$$\tan\phi = \left|\frac{d}{dr}W(a)\right| = \frac{2W_m}{a} \tag{3.6}$$

Using some basic trigonometry it can be shown that

$$\sin\phi = \frac{2W_m}{\sqrt{a^2 + 4W_m^2}} \tag{3.7}$$

The magnitude of the tension in the out of plane direction is:

$$\left|\tau_z\right| = \tau \sin\phi \equiv \frac{2\tau W_m}{\sqrt{a^2 + 4W_m^2}} \tag{3.8}$$

This out of plane component of tension is the amount of pull that is being experienced at the adhesive interface. As pressure increases, deflection of the membrane increases along with the angle of deflection ϕ. Deflection will continue to increase with increasing pressure until the magnitude of the out of plane tension exceeds the strength of the adhesive. This critical tension is τ^c, and is the maximum amount of tension that the adhesive can hold. This is one of the failure criteria. So $|\tau_z| = \tau^c$ at the critical pressure, or put another way:

$$\tau^c = \frac{2\tau W_m \lambda_c}{\sqrt{a^2 + 4W_m^2}} \tag{3.9}$$

The deflection at the critical pressure is

$$W_m(\lambda_c) = \left(\frac{a^2}{4\tau}\right)\lambda_c \tag{3.10}$$

This can be rearranged to show

$$\lambda_c = \frac{2\tau^c}{a\sqrt{1-\left(\frac{\tau^c}{\tau}\right)^2}} = \frac{K(\rho,\tau,\tau^c)}{a} \tag{3.11}$$

The critical pressure of delamination there is a function of initial defect radius a, tension in the membrane τ, and critical tension between the elastic membrane and adhesive τ^c.

Simple Griffith Criterion

The next model still employs the membrane deflection equation, but rather than use a force (or tension) balance to predict the pressure of delamination, an energy balance of the debonded membrane system is used. This approach assumes that the state of stress

and strain of the deflected membrane is the same in both the axial and radial directions. The net energy expended to deform the membrane is given by:

$$\Pi_a = -\frac{1}{2}\iint_{R_a}\left\{\tau\left|\nabla W\right|^2 - 2\lambda W\right\}dA \tag{3.12}$$

Since the blister is axisymmetric $R_a = \left\{(r,\theta)\middle| 0 \le r \le a, 0 \le \theta \le 2\pi\right\}$, and the differential operator is given by $\left|\nabla W\right|^2 = W_{,r}^2$. Since $W_{,r} = -\frac{\lambda r}{2\tau}$, (3.12) can be rewritten as:

$$\Pi_a = -\frac{1}{2}\iint_{R_a}\left\{\frac{\lambda^2}{4\tau}r^2 - \frac{\lambda^2}{2\tau}(a^2 - r^2)\right\}dA \tag{3.13}$$

Integration of the net energy in (3.13) produces:

$$\Pi_a = \frac{\pi\lambda^2 a^4}{16\tau} \tag{3.14}$$

The Griffith criterion indicates that the crack will propagate if the energy release rate exceeds a critical value; this is known as the critical energy release rate G_a*. Where the energy release rate is defined by:

$$G \equiv \frac{\partial \Pi_a}{\partial a} \tag{3.15}$$

The critical energy release rate is a constant value for this system; it is the amount of energy necessary to create a new surface area. Once the work done on the system exceeds this value the crack will propagate. By equating (3.15) to G_a one can find the critical pressure (3.16).

$$\lambda_c = \frac{2\sqrt{2\tau G_a}}{a} \tag{3.16}$$

* This is also known as the adhesive toughness. Adhesive toughness is most appropriate for the experimental set up involved with this work.

Griffith Criterion with Radial Strain

The third model also uses the Griffith criteria from fracture mechanics, but this model differs from the previous model in that it takes the radial strain into account. The simple Griffith utilizes the assumption that the strain is the same thought the membrane, while the third approach is somewhat more generalized.

The starting point for this model is a coupled system of differential equations from plate theory, where w=w(r,t) is the displacement, and Φ=Φ(r,t) is the Airy stress function; which describes the state of stress in the body, and ρ is the density of the material.

$$\rho \frac{\partial^2 w}{\partial t^2} - K\Delta^2 w = [\Phi, w_o + w] + \lambda \tag{3.17}$$

$$\frac{1}{Eh}\Delta^2 \Phi = -\frac{1}{2}[w, w] - [w_0, w] \tag{3.18}^{\dagger}$$

Where the bending stiffness is given by:

$$K = \frac{Eh^3}{12(1-\nu^2)} \tag{3.19}$$

For a membrane, the bending stiffness is negligible K≈0. If $u_{,r}$ is the radial displacement of the membrane, then the net strain energy and potential energy expressions are given by:

$$U_a = \frac{\pi Eh}{1-\nu^2}\int_0^a \left\{ \left(u_{r,r} + \frac{1}{2} w_{,r} \right)^2 + 2\nu \left(u_{r,r} + \frac{1}{2} w_{,r}^2 \right) \frac{u_r}{r} + \left(\frac{u_r}{r} \right)^2 \right\} r \cdot dr \tag{3.20}$$

---

† Some Notes on notation, Bracketed variables are multiplicative derivatives

e.g $[f, g] = f_{,yy} g_{,xx} - 2 f_{,xy} g_{,xy} + f_{,xx} g_{,yy}$

and the Biharmonic operator Δ is given by

$$\Delta^s w = \frac{\partial^4 w}{\partial x^4} + 2\frac{\partial^4 w}{\partial x^2 \partial y^2} + \frac{\partial^4 w}{\partial y^4}$$

$$V_a = 2\pi\lambda\int_0^a wr \cdot dr \tag{3.21}$$

The total energy of the system is $\Pi_a = U_a + V_a$.

The full derivation is rather laborious and involved, and is included in Appendix D. From that work it is shown that:

$$\Pi_a = \frac{\pi Eh}{1-\nu^2}\int_0^a \left\{A + B\lambda r + C\lambda^2 r^2\right\} r \cdot dr + 2\pi\lambda^2 D\int_0^a \left(a^2 - r^2\right) r \cdot dr \tag{3.22}$$

Where the coefficients are:

$$\begin{cases} A = \dfrac{(1+2\nu)}{(1+\nu)^2} \\ B = \dfrac{-(1-\nu)}{2Eh} \\ C = \dfrac{(1+9\nu)}{16(1+\nu)}\dfrac{(1-\nu^2)^2}{E^2h^2} \\ D = \dfrac{(1-\nu^2)}{4Eh} \end{cases} \tag{3.23}$$

Integrating (3.22) produces the following expression (3.24)

$$\Pi_a = \frac{\pi Eh}{1-\nu^2}\left(\frac{1}{2}Aa^2 + \frac{1}{3}B\lambda a^3\right) + \frac{\pi}{4}\left(\frac{Eh}{1-\nu^2}C + 2D\right)\lambda^2 a^4 \tag{3.24}$$

Then employing the Griffith criterion that is taking the derivative of the total energy of the system the following expression can be found.

$$\frac{Eh}{2(1-\nu^2)}\left\{A + B\lambda_c a + C\lambda_c^2 a^2\right\} + D\lambda_c^2 a^2 = G_a \tag{3.25}$$

This expression is not as simple as the two previous models; it requires an iterative solution to find the critical pressure. Engineering Equation Solver (EES) was employed to calculate the values for this model. The results of these calculations can be seen in Appendix A.

There are three models that have been presented in this chapter; they are summarized in Table 3-1. The first two models indicate that the critical pressure will be inversely proportional to the initial defect radius. While the Griffith criterion which takes strain into account is not so easy to say what behavior it will exhibit, it seems appropriate that a decrease in critical pressure will occur for increasing the size of defect. Intuitively this is appealing because it makes sense that a sheet with a large defect would take less effort to blister than would a sheet with a smaller defect. The following chapters will discuss the experimental work that was employed to validate the models.

Table 3-1: Failure Criteria for Delamination

Eq	Failure Criteria
(3.16)	$\lambda_c = \frac{2\tau^c}{a\sqrt{1-\left(\frac{\tau^c}{\tau}\right)^2}}$
(3.11)	$\lambda_c = \frac{2\sqrt{2\pi G_a}}{a}$
(3.25)	$\frac{Eh}{2(1-\nu^2)}\left\{A + B\lambda_c a + C\lambda_c^2 a^2\right\} + D\lambda_c^2 a^2 = G_a$

Chapter 4 Methodology

Elastic Properties of Latex

The goal of this experiment was to understand the elastic properties of the latex sheets used for the critical pressure experiment, so that a specimen can be pre-tensioned to a known value. A series of tensile tests were conducted on the latex sheets. The data from this experiment was relevant to the strain used in the critical energy release rate; as well as the amount of tension that was put in the elastic membrane prior to the critical pressure experiment. The specific interest was to locate a linear region of elasticity for these samples. The ultimate goal was to accurately know how much stress was developed in a sheet for a given amount of strain; and to ascertain the degree of certainty of these results.

Theory/Equation

It is assumed that the only mode of loading is along the direction of pull experienced from the tensile tester. It follows that the stress present in the tensile specimen is simply the load over the cross-sectional area of the specimen.

$$\sigma = \frac{F}{A_c} \tag{4.1}$$

Where F is the load from the tensile tester, and A_c is the cross-sectional area. The cross-sectional area of the specimen is:

$$A_c = h \cdot b \tag{4.2}$$

Where h is the thickness and b is the width of the elastic specimen, respectively.

Apparatus

The tensile tester was an Instron 1122, which uses Instron Series IX software for data acquisition, shown in Figure 4.1.

Figure 4.1: Instron 1122 used for Tensile Tests

Procedure

ASTM D412-98a was followed to test the tensile specimens. The specimens were cut into 7.62 cm x 2.54 cm strips. A pull rate of 8.47 mm/s was used on the Instron 1122. A 2.54 cm gauge length was utilized for the test. The thickness of the gauge length was then measured. The measurements were taken with an Emveco 200A-Electronic Microgage.

The Series IX DAQ, software collected data for analysis. Method 84 was the software protocol used, in accordance with ASTM D412-98a. After the load cell was calibrated, three sheets were tested, for a total of 54 test specimens.

Critical Tension & Critical Energy Release Rate

In order to make theoretical predictions based on the mathematical model the critical energy release rate and critical tension were needed. These quantities are unique to the combination of latex and epoxy of our experiments.

Theory/Equation

The equations predicting critical pressure depend on the initial tension in the membrane, that is, the membrane is tensioned before pressure is applied. As pressure is applied the membrane deflects. Deflection continues until a critical value is reached where delamination begins, this is called the critical pressure. τ^c is the vertical component of tension in the membrane when delamination occurs. Put another way, as the pressure deflects the membrane, the bond of the latex is no longer able to hold the vertical component of tension; this critical value for τ_z is known as τ^c.

For the two Griffith models, the critical energy release rate, G_a, was found using the peel test. Critical energy release rate is the resistance of the bond to failure, it is the amount of energy needed to create a unit of new surface, it is an inherent property of a given system; much the same way fracture toughness is a property inherent to a given material.

The elastic membranes used in this work were extensible and have negligible bending stiffness. The critical energy release rate of an extensible, flexible membrane is given by (2.2):

$$G_a = \frac{F_c}{b}\left(1 - \cos\theta + \frac{\varepsilon}{2}\right) \tag{2.2}$$

Where F_c is the load required to peel the membrane from a rigid substrate, b is the width of the specimen, θ is the angle of peel, and ε is the strain in the membrane when peel initiates.

The critical tension, on the other hand, is simply the tension at which the bond between the membrane and the adhesive fails. It can be simply defined as:

$$\tau^c = \frac{F_c}{b} \tag{4.3}$$

The difference in the two formulations is somewhat subtle. The method of critical tension is based upon a force balance of the system. The failure criterion is based on the vectorial component that is necessary to break the adhesive bonds of the glue. The Griffith criterion is based on the overall energy balance of the system. As such the models using the Griffith criterion take the strain of the elastic membrane into account directly.

To find these critical values a set of peel tests were performed. Figure 4.2 shows a schematic of the peel test.

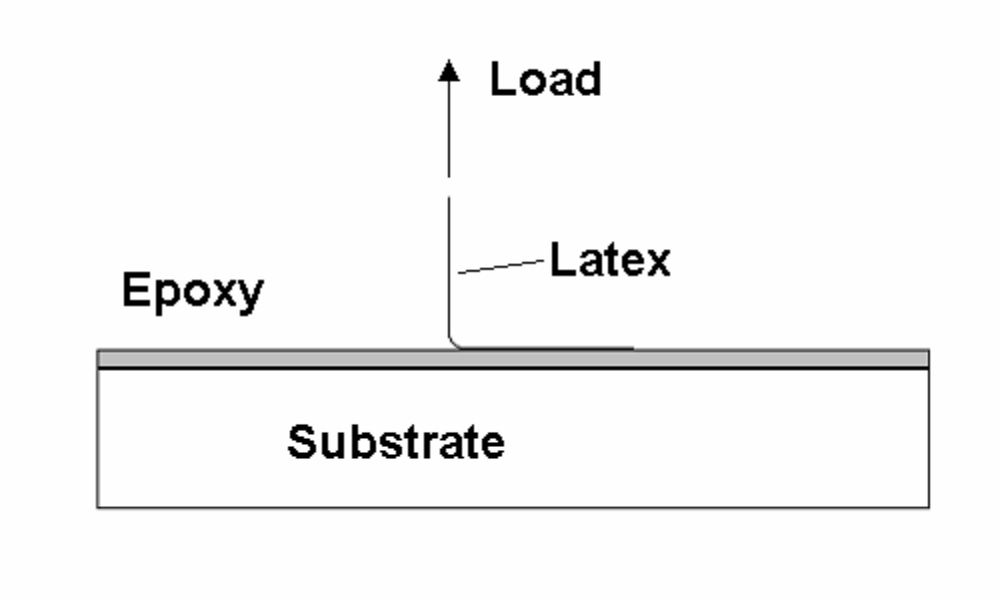

Figure 4.2: Peel Test Schematic

The material exhibits two distinct behaviors in this test, stretch and peel. Stretch is the initial elongation in the membrane before it begins to peel. Peel follows immediately after some critical load is reached; in this case F_c. There are two distinctly different slopes on a force-displacement diagram. The point where the slope change occurs is F_c, it signifies when peel initiates. The two regions are shown schematically in Figure 4.3; note the elastic stretch region and a nearly constant force peel region. In the experiment, the angle of peel in the test was nearly vertical, so the cosine term in (2.2) can be neglected. The critical energy release rate may then be written as:

$$G_a = \frac{F_c}{b}\left(1 + \frac{\varepsilon}{2}\right) \tag{4.4}$$

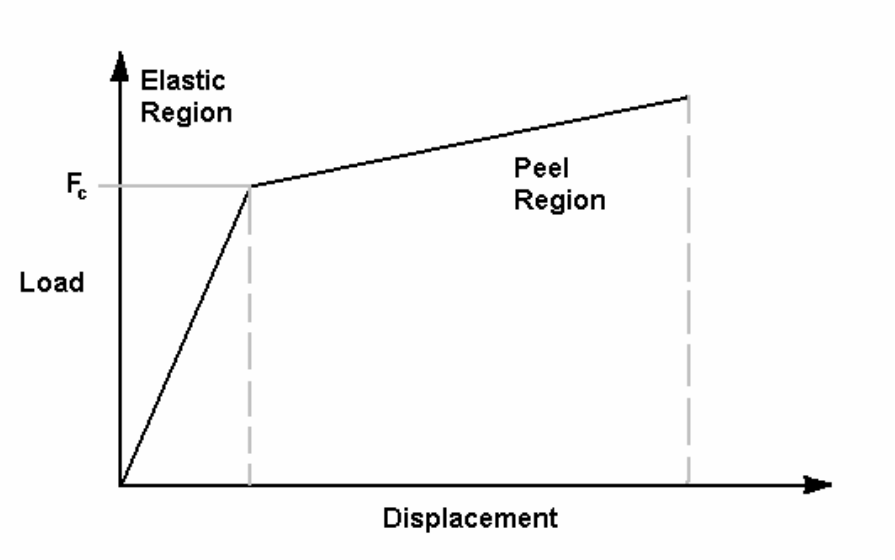

Figure 4.3: Schematic of Peel Test Output

Apparatus

The rigid substrate was a 1.27 cm x 10.16 cm x 15.24 cm stainless steel plate, as shown in Figure 4.4. The plate was marked with a 2.54 cm wide strip that represents the test area of interest where the elastic was peeled back from the epoxy layer. The plate was drilled with a bolt-hole pattern to rigidly attach it to the tensile tester.

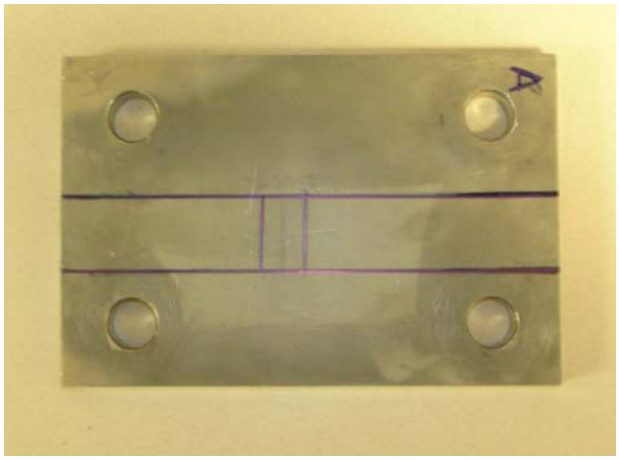

Figure 4.4: Stainless Steel Substrate

The tensile tester was an Instron 1122, which uses Instron Series IX software for data acquisition, a peel test in progress is shown in Figure 4.5.

Figure 4.5: Peel Test

Procedure

The elastic material membrane was 15.24 cm x 25.40 cm latex sheets. They had an average thickness of approximately 0.0931 mm. The thickness varied slightly across the width, so it was necessary to measure the thickness of each specimen prior to any test. These sheets were cut into 5.08 cm x 10.16 cm strips for testing purposes. The strain in the strip was found using Hooke's Law. The next chapter will present the constitutive relationship for the peel test. Accordingly, the thickness of the specimen must be taken into account also when calculating the stress and strain in the test strips.

The elastic strips were glued to the substrate and allowed to cure for at least one hour, according to the epoxy manufacturer's specification. The membrane and substrate were bolted to the crosshead of the Instron and the loose end of the membrane was

secured in the load-cell clamp. The same software protocol that was used for the tensile test was used for the peel test. A crosshead speed of 0.2 mm/s was used instead, because it has been suggested that this is close to the rate of crack propagation for this system.

Critical Pressure

The critical pressure must be evaluated experimentally, which was the goal of this experiment. Data from this experiment was then used to evaluate the different mathematical models. The basic concept was as follows, air pressure was applied to the system; the fluid exerts hydrostatic pressure on the membrane. The pressure was slowly increased step-wise until delamination of the membrane occurs.

Apparatus

The apparatus consisted of a pressure source, regulator, fluid reservoir, and the substrate; a schematic of the experimental set up can be seen in Figure 4.6 and a picture of the apparatus can be seen in Figure 4.7.

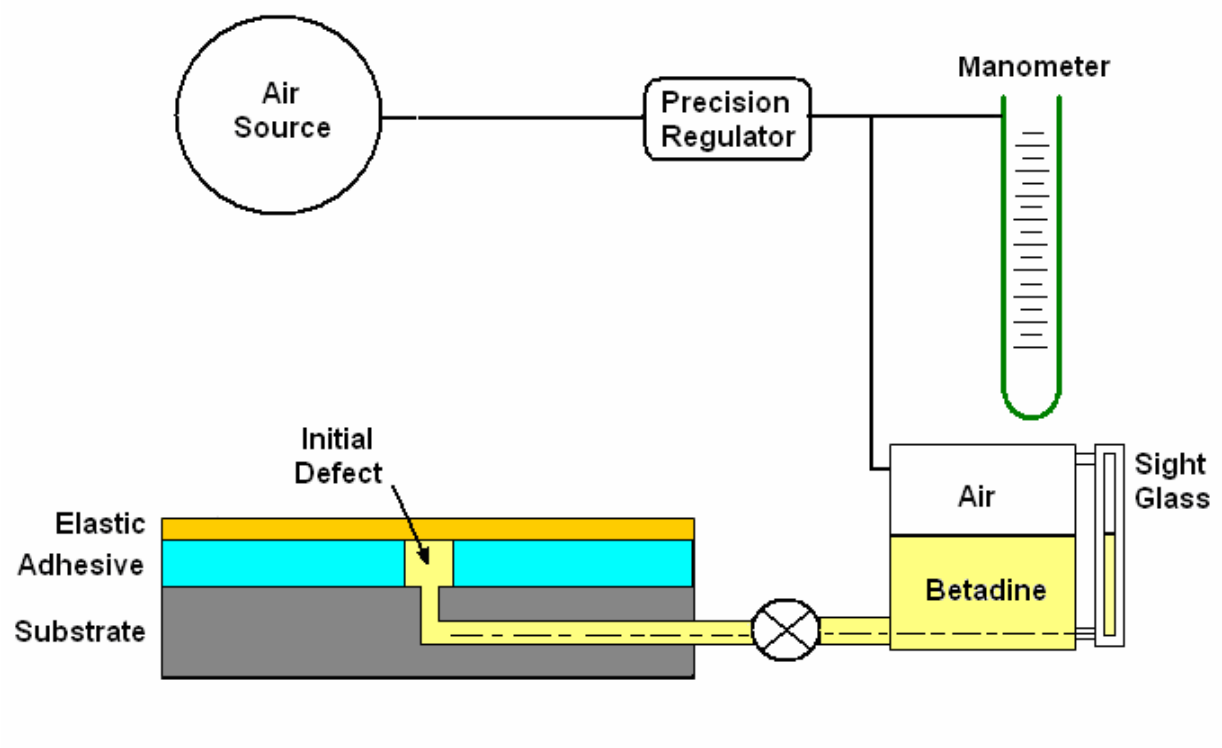

Figure 4.6: Critical Pressure Experiment Schematic

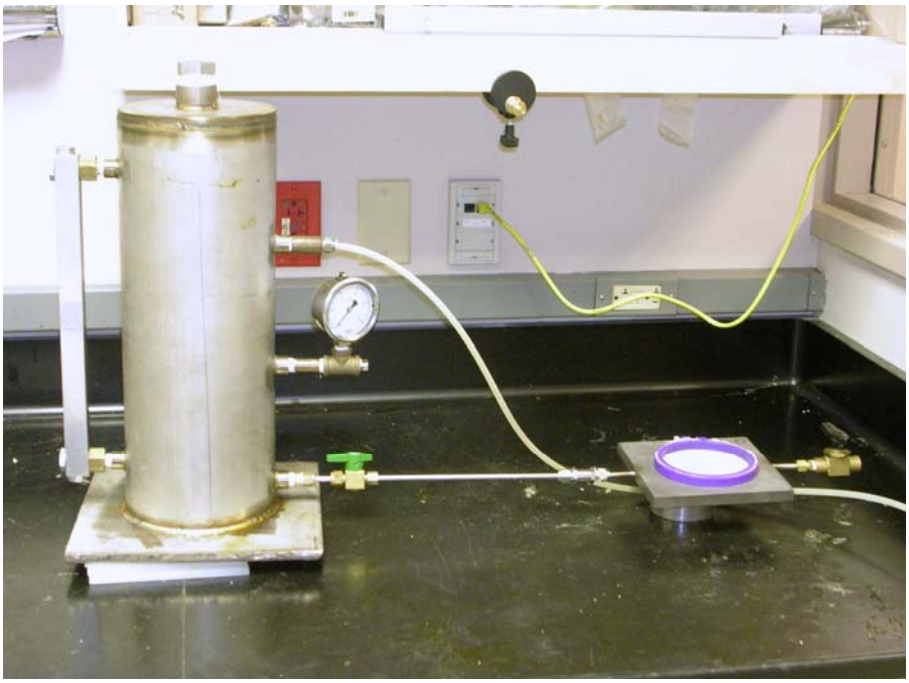

Figure 4.7: Critical Pressure Apparatus

The pressure source was the in-house high pressure air supply. Air pressure was regulated with a primary regulator at approximately 172 kPa. This primary pressure was

stepped down with a precision regulator, a ControlAir high precision regulator; it has an accuracy of 0.1% between the 0 to 103 kPa. This range was well within the limits of this experiment. A Dwyer manometer was used to measure the amount of static pressure supplied to the fluid reservoir.

The fluid reservoir can be seen in Figure 4.8. The reservoir was filled with a 10% USP Iodine solution (betadine) to aid in visual inspection of crack propagation. The iodine was found to have the most easily discernible visual contrast; this is important for the image analysis portion of the analysis. The sight glass was used to measure the fluid head pressure exerted by the iodine on the membrane.

Figure 4.8: Fluid Reservoir

Pressure at the defect was the sum of the air pressure at the manometer and the pressure from the fluid head. The equation to calculate the pressure at the defect is:

$$\lambda_{\text{defect}} = \gamma(z_m + z_f) \tag{4.5}$$

Where z_m and z_f are the height of the fluid head of the manometer and fluid reservoir, respectively; and γ is the specific weight $\gamma=\rho g$. The densities of the two fluids were identical to water, so they have the same γ.

Four stainless steel plates were used as substrates for this experiment; the plates are shown in Figure 4.9. The substrates were polished stainless steel plates which had holes of radii 3.18 mm, 4.77 mm, 6.35 mm, and 7.94 mm. It should be noted that these radii were not the same as the defect radii. The initial defect radii were determined by the geometry of the cured epoxy; this is discussed further in the image analysis section.

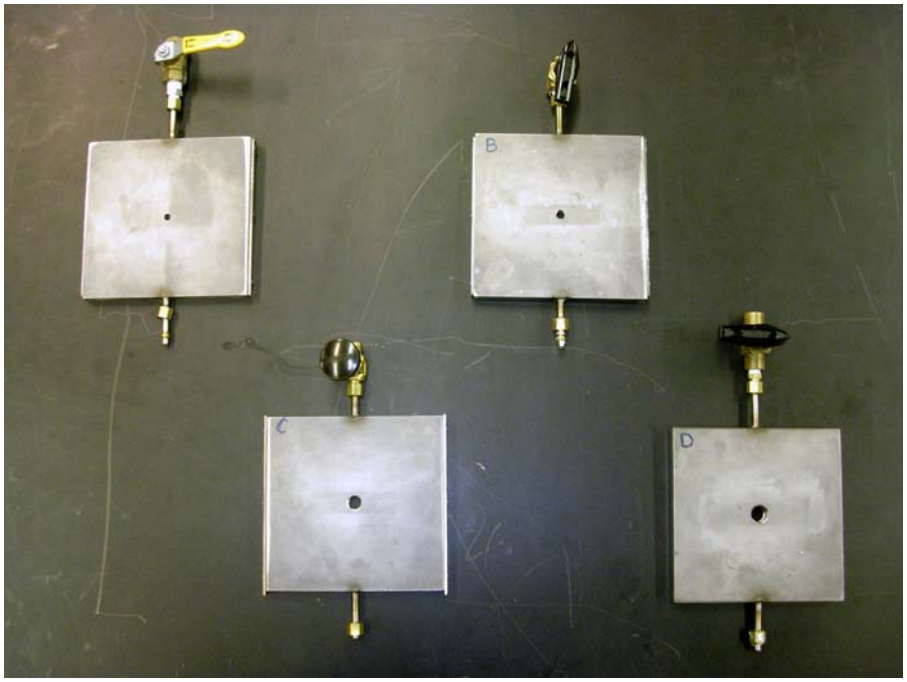

Figure 4.9: Critical Pressure Plates

Procedure

As already indicated the membranes had to be pre-tensioned before they could be glued to the plate. This was accomplished by marking a 2.54 cm square on the membrane. This membrane was then stretched over a right circular cylinder and clamped

securely. The new dimensions of the square were measured and the strain calculated. The constitutive relationship of latex for this strain range could then be used to find the stress and tension in the membrane. It was assumed that the thickness of the membrane was the mean sheet thickness (0.0931 mm). The tension in the membrane was the stress multiplied by the thickness, that is, the load per unit width in the membrane. A pre-tensioned membrane is shown in Figure 4.10.

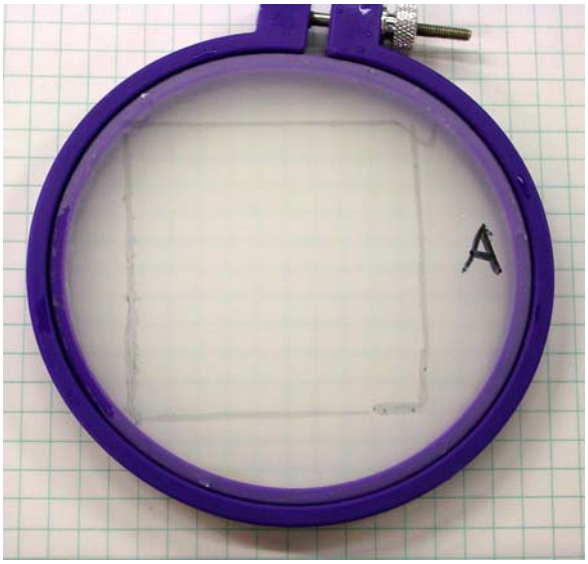

Figure 4.10: Pretensioned Elastic Membrane

The samples were cleaned with sudsy water and rinsed with distilled water prior to gluing. This was done to remove any foreign material that might interfere with the adhesive bond between the latex and epoxy. Epoxy was placed on the substrate as close to the hole in the plate as possible; without entering the hole. The clean, pre-tensioned membrane was placed on the substrate and allowed to cure for one hour. At this point, sample preparation was complete and the test was ready to proceed.

The initial iodine head was measured. The pressure was increased slowly stepwise, observing the sample. The process was quasi-static, so each sample stayed at each pressure step for at least 120 seconds. Pressure was increased in this way until

delamination occured. Figure 4.11, shows a delaminating membrane. Once delamination occured, pictures were taken for image analysis. A synopsis of the image analysis procedure is given in Appendix C.

Figure 4.11: Elastic Membrane Delaminating

Perforation Test

The pressurized blister tests were useful, as they allow us to observe the effect of initial defect size on the critical pressure of delamination. However, these tests are useful for a closed system only, and the pores in paper are not isolated. Paper, especially wet paper, is a complex network of fibers forming interconnected pores of various sizes. These pores are very often not isolated, and consequently steam expansion in an impulse dryer is not contained explicitly within the domain of the pore. Some of water that flashes to steam leaves the pore and travels through the web. Work was done to assess the effects of these pore networks.

The goal of these experiments was to understand what effect escaping gas and an open system would have on the critical pressure of the system. Two tapes were used on the stainless steel substrates used for the critical pressure tests, and the effects of perforations were tested.

Apparatus

Two plastic tapes were used for this work. It was necessary to use a different material because the latex membranes used to validate the models had a high propensity to rupture when a perforation was introduced. The two tapes used were Clear 3M and UL black electrical tape.

The same stainless steel substrates, Figure 4.9, that were used for the critical pressure experiments were employed for this work. The surface properties of the plate were much more important for this case, because the thickness of the tape was much thinner than the epoxy used with the latex membranes. Consequently the plates were polished with a lapping machine, so that there was only a maximum 0.102 cm variation possible across the surface of the surface. Additionally, the same system for testing the critical pressure of the latex system, Figure 4.6, was used for this test. The tape specimens were not tensioned.

Procedure

Two sets of tests were run on the tape specimens. A set of non-perforated test were run as a baseline to compare the perforated tests against. The idea here was to quickly understand the effect of the perforations on the critical pressure of the blisters.

The non-perforated test was conducted first. Tape was placed on clean substrates, and pressurized in a similar manner to the previous critical pressure tests were. The tape

was applied to each of the plates. Initial defect radii were the same as the holes in the plate (3.18 mm, 4.77 mm, 6.35 mm, and 7.94 mm) , because there was no variability with the adhesive. The values of delamination were tabulated and are presented in Chapter 5.

Perforated tests were carried out after next. Tape was applied to a clean substrate, and then a soldering iron with a very sharp point was used to perforate the tape. Pictures were taken of the perforations and the procedure described in Appendix C was used to find the size of the perforation. Again, the same procedure of ramping the pressure up step-wise was used until delamination occurred.

Chapter 5 Results and Discussion

Thickness Gradient

Figure 5.1 shows the change in thickness for the sheets of latex as they were received. The thickness varied from 0.0663 mm to 0.1183 mm. This change in material thickness was found to vary only across the width of the sheet, so that there were lanes of near uniform thickness throughout the length of the sheet. The variation in latex thickness has a strong linear correlation.

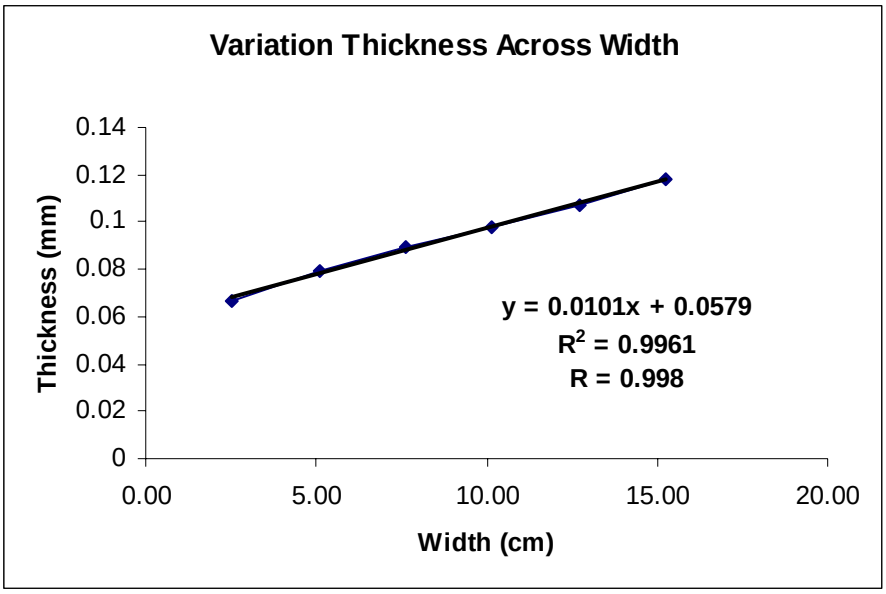

Figure 5.1: Variation of Thickness for Latex Sheets

Figure 5.2 shows a representation of the overall thickness gradient for the sheets. It is clear from this figure that the thickness does not change with the length but only along the width. These lanes of relatively uniform thickness are important in the tensile test section of this thesis, as we need the cross-sectional area of the tensile specimens.

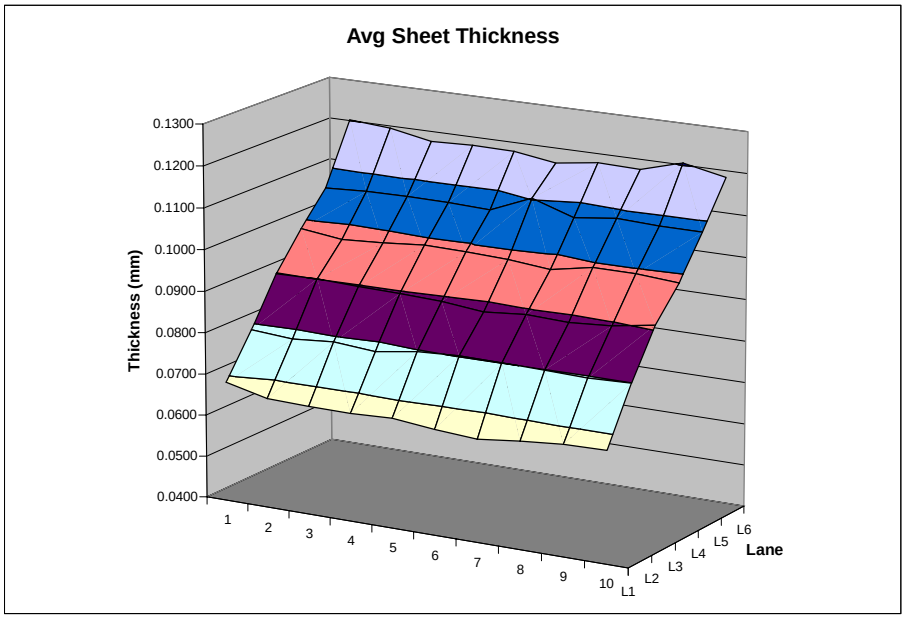

Figure 5.2: Variation of width throughout latex sheets

Elastic Behavior

The results of the tensile tests are shown in Figure 5.3. Shown is the average of 54 tensile tests. This is the overall elastic response of the strip. This material is capable of high strains; as one would expect from latex. There are also distinct linear regions present.

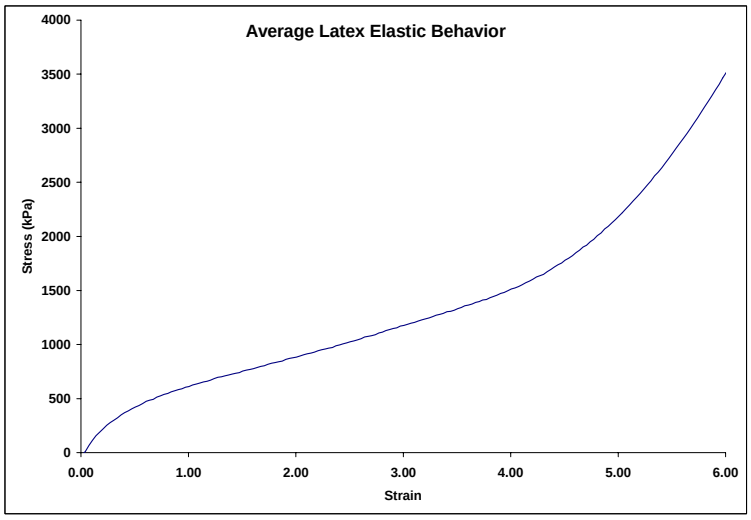

Figure 5.3: Overall Elastic Behavior of Latex Sheets

There are two regions of particular interest, the linear regions between strains of 0.0 and 0.51, and strains between 1.0 and 4.0. The first region governs the elastic behavior in the peel test; the stress values represent the range of stresses exhibited in that test, and Figure 5.4 shows the tensile region for the peel test. The latter region is used to pretension the membrane for the critical pressure experiment, and Figure 5.5 shows this region.

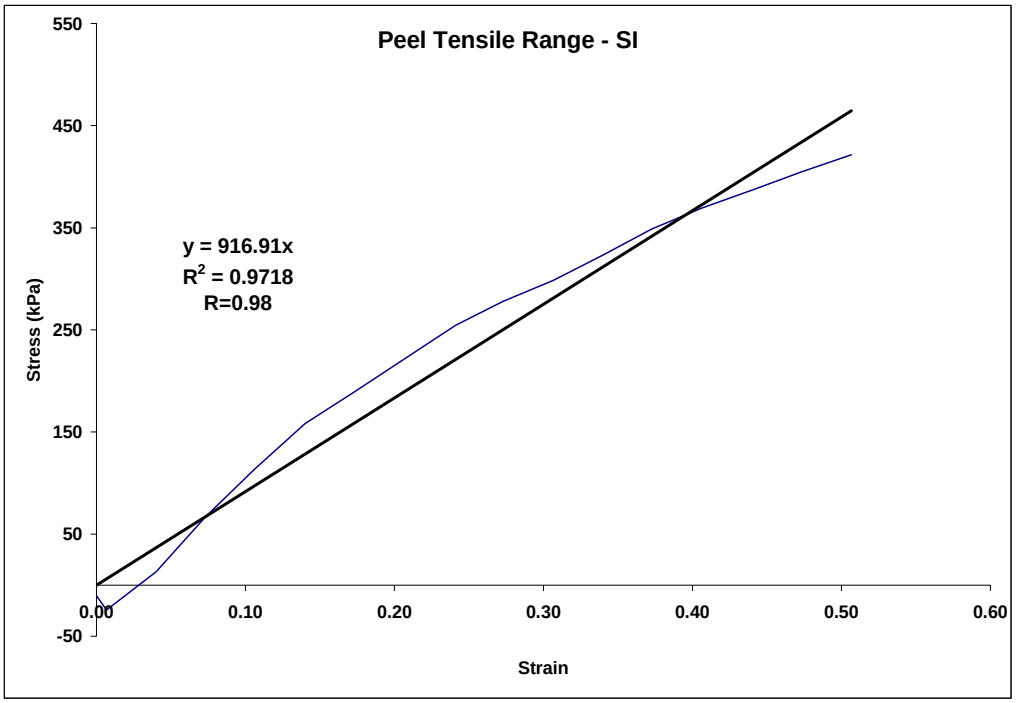

Figure 5.4: Linear Tensile Range for Peel Tests

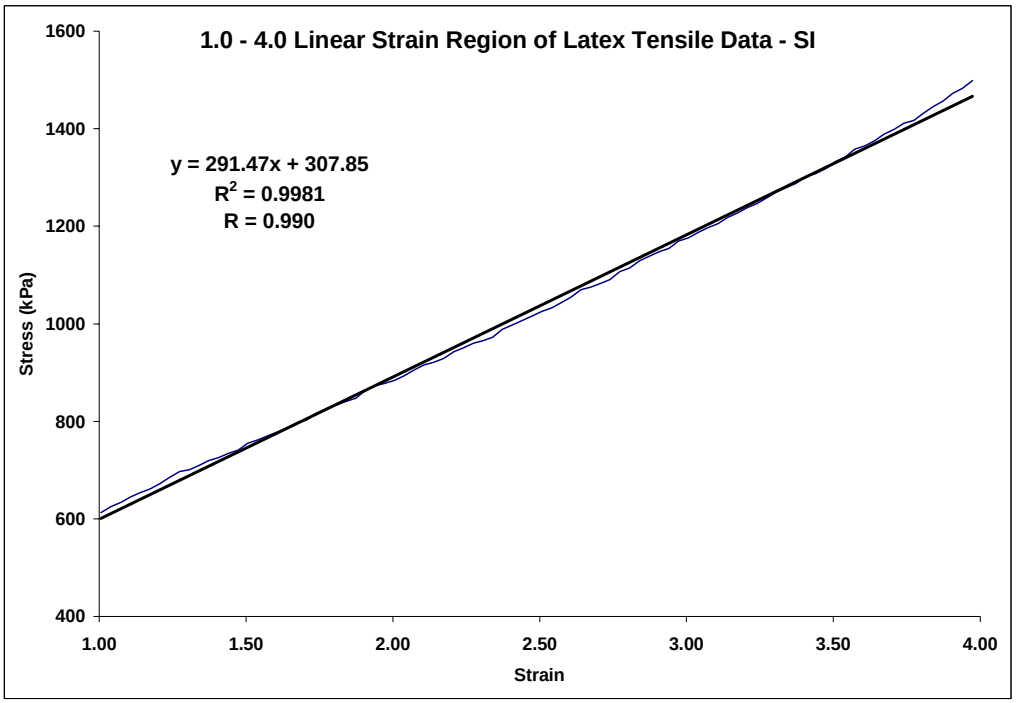

Figure 5.5: Linear Tensile Range for Tensioning Elastic Membranes

Poisson Ratio

The Griffith model which takes radial strain into account is dependent upon the poisson ratio of the elastic membrane, so it was necessary to measure this for the material used. The Poisson ratio is defined as:

$$\nu = -\frac{\varepsilon'}{\varepsilon} \tag{5.1}$$

Where ε is the strain in the normal direction and ε' is the strain in the transverse direction. Six specimens were tested with little or no distinguishable difference in any of the specimens. The Poisson ratio was found to be 0.24.

Peel Test

A total of 24 points were taken for the data set of the peel tests. One of these was discarded, because it lay outside of the 95% confidence interval. Figure 5.6 shows the

results of one of these tests. Note how a clear change in slope is readily apparent in Figure 5.6.

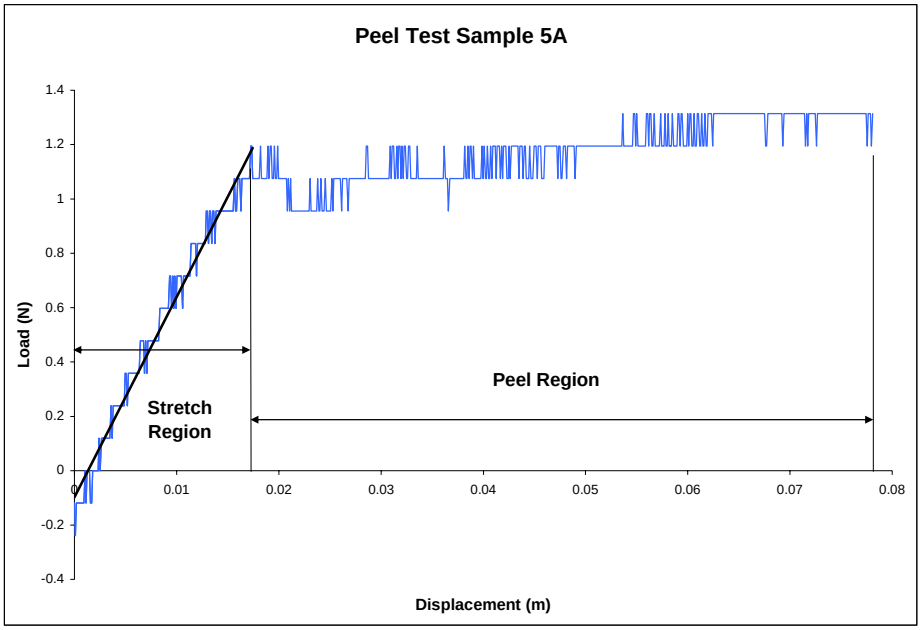

Figure 5.6: Peel Test Example

Equations (4.3) & (4.4) were used to calculate the critical tension and critical energy release rate, respectively. The critical force was used to find the state of stress and strain in the body. Sample calculations are given in Appendix B. The resultant data set is summarized in Appendix A. The mean values and standard deviations of the data set are given in Table 5-1.

Table 5-1: Peel Test Results

	G_a (N/m)	τ^c (N/m)
Mean	33.36	28.79
St. Dev.	9.03	7.11

Critical Pressure

The theoretical and experimental results are shown in Figure 5.7. As expected, the pressure is inversely proportional to the initial defect radius.

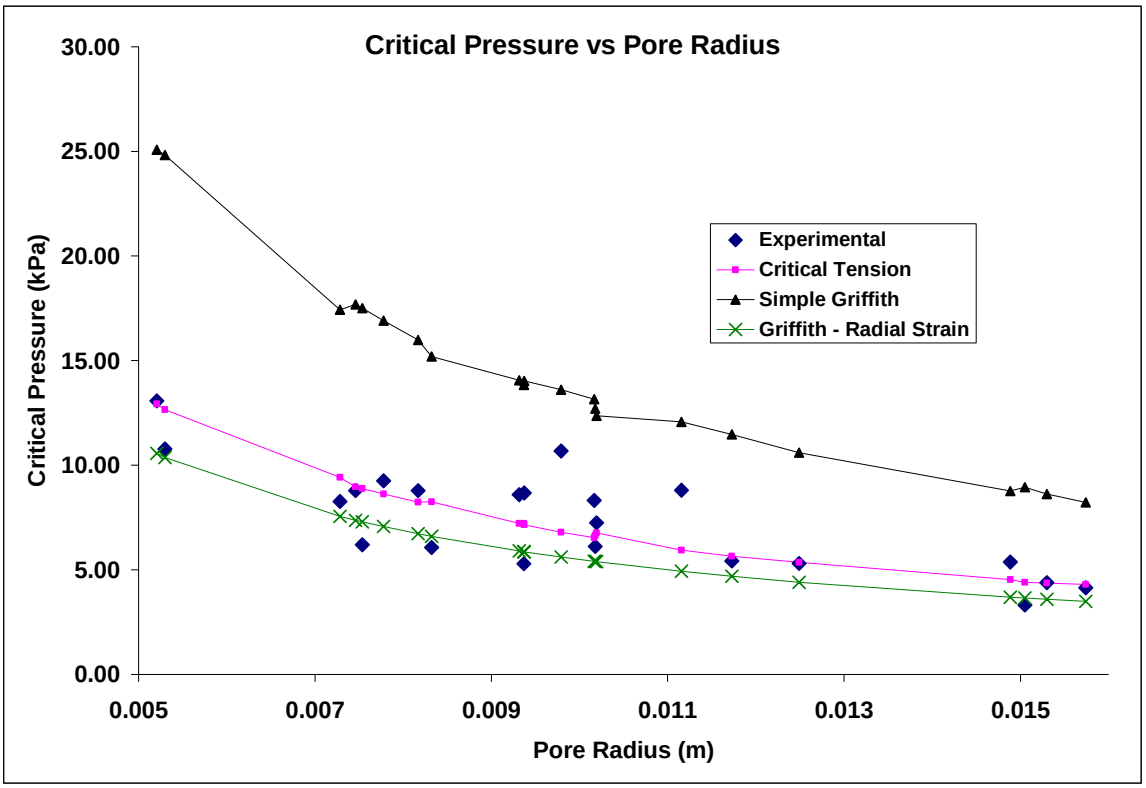

Figure 5.7: Comparison Experimental and Theoretical Critical Pressures

Of these approaches the Griffith Criterion that takes the radial strain into consideration is the best fit for the data. The critical tension follows closely behind, and the simple Griffith model being the poorest fit of the data.

Perforation Test

Shown in Figure 5.8, are the results of the perforation test for the black tape, and Figure 5.9 shows the effect on the clear tape specimens. These are average values, three data points were found for each; these data sets are given in Appendix A. The critical pressure, as expected, was inversely proportional to the initial defect radius for both the

black tape and the clear tape. Additionally, the samples with perforations all have higher critical pressures.

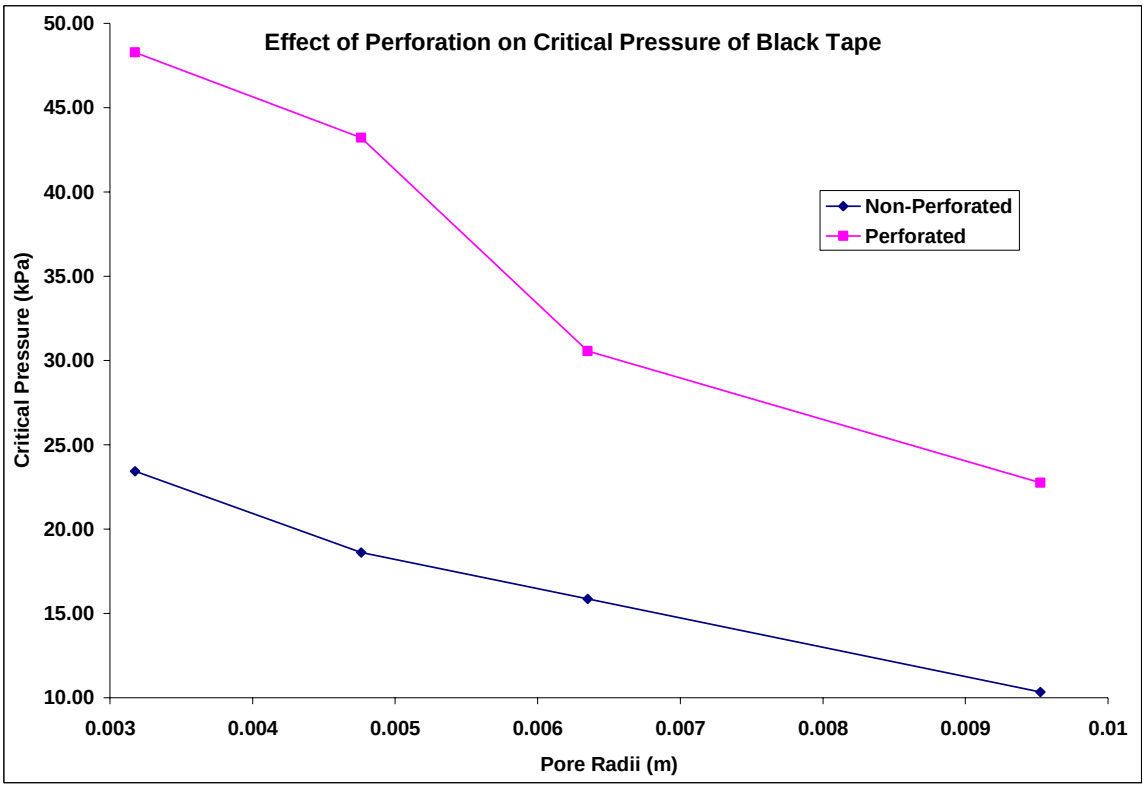

Figure 5.8:Results of Perforation on Delamination of Black Tape

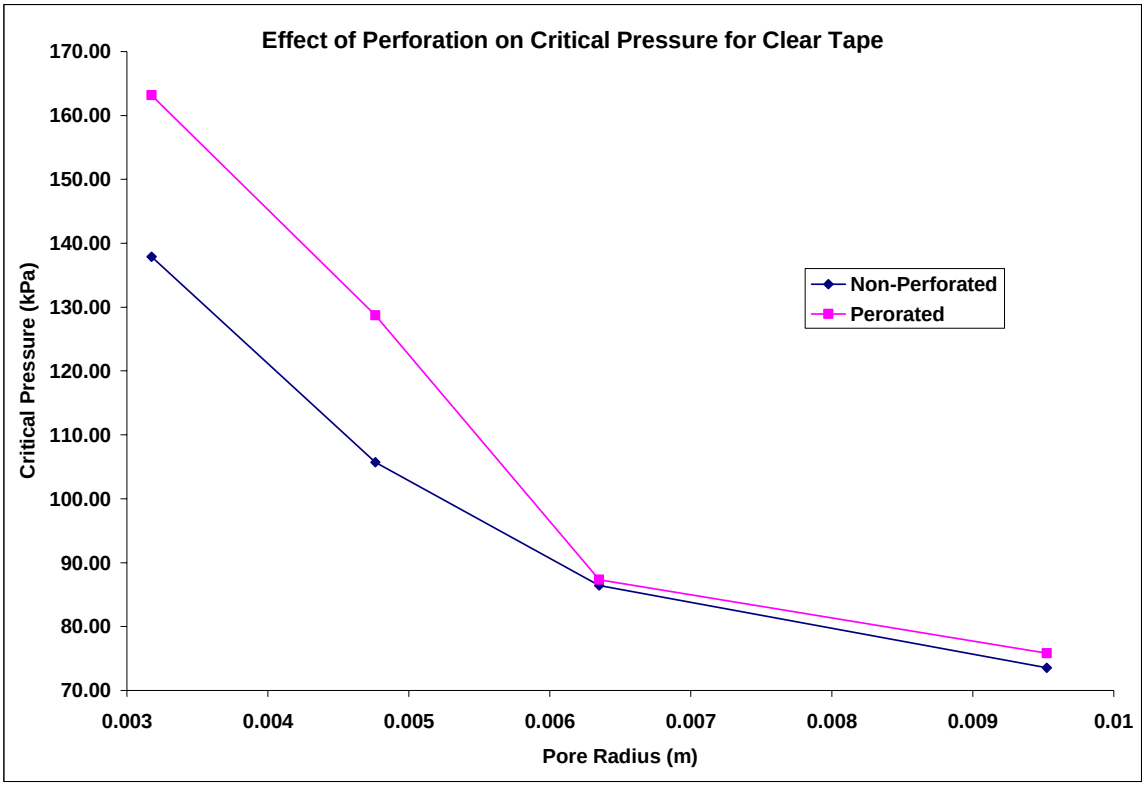

Figure 5.9: Results of Perforation on Delamination of Clear Tape

A possible explanation for this higher pressure could be that for a given defect radius there is a given force that is needed to initiate delamination, where the force is the applied pressure times the surface area, A_s:

$$F_c = \lambda_c A_s \Rightarrow \lambda_c = \frac{F_c}{A_s} \tag{5.2}$$

This force should be a constant for a given initial defect system. For a non-perforated system the surface area is greater than that of the perforated system, so the critical pressure necessary to achieve this critical force must be higher to induce delamination of the elastic membrane.

This critical force was found for the non-perforated tests for both the black tapes and the clear tapes at their varying initial defect radii. A prediction of the values for the

perforated samples was then calculated using (5.2); the surface area was assumed to be a spherical dome with a circular perforation. The results of the analysis are shown in Figure 5.10 for the black tape and Figure 5.11 for the clear tape. The figures compare the critical pressures for non-perforated, perforated, and geometric effects. The geometric effects almost match up with the non-perforated results. From Figure 5.10, it appears that the geometric effect almost able to describe the higher critical pressures. However, for the clear tape the geometric effects do not fully account for the observed phenomena.

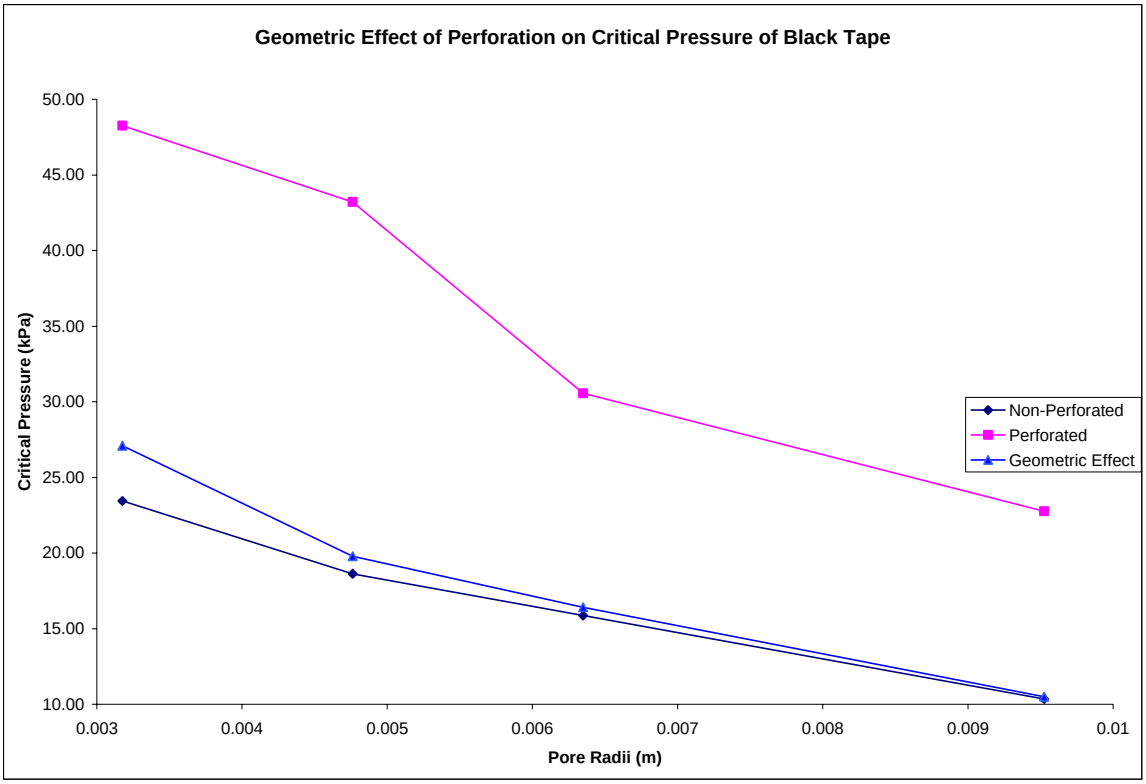

Figure 5.10: Results of Perforation Test Including Geometric Effect for Black Tape

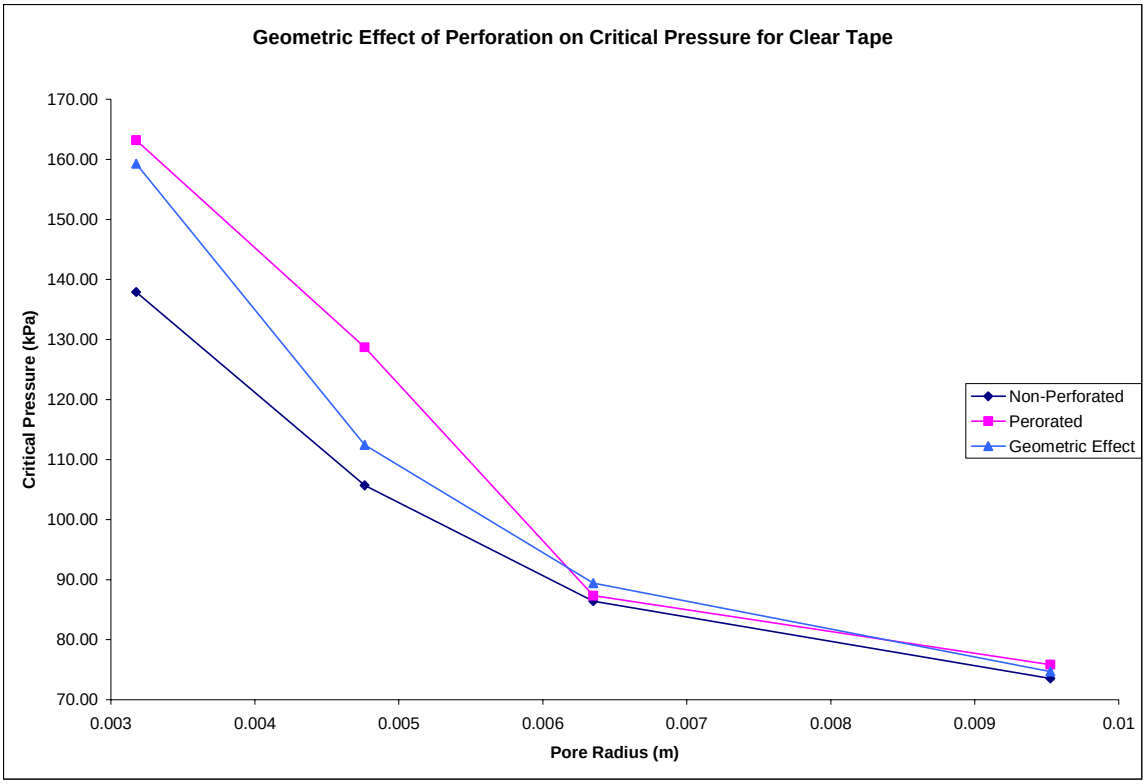

Figure 5.11: Results of Perforation Test Including Geometric Effect for Clear Tape

Chapter 6 Conclusion and Recommendations for Future Work

A set of models have been proposed to describe delamination of an elastic system. The purpose of the models was to shed light on the more complex delamination of wet paper upon exiting the nip of an impulse dryer.

The models used a membrane equation to describe deflection of the initial defect. Three failure criteria were imposed on the membrane equation. The critical tension model used a force balance to predict when the blister would begin to peel. The simple Griffith model used an (LEFM) approach that assumed stress throughout the deflected membrane was uniform. The Griffith model, which took radial strain into account, was the third model. The critical tension and simple Griffith model predicted that the critical pressure would be inversely proportional to the initial defect.

Blister tests were conduced to test these theories. The experimental results were compared to the results from the theoretical models. The Griffith approach, which included radial strain appears to be the best overall fit of the data. The critical tension model was also a close fit. The simple Griffith model provides the poorest fit to the data. As predicted, the critical pressure was experimentally found to be inversely proportional to the initial defect radius. Webs with higher levels of refinement, smaller pores, will be less likely to delaminate. Thus smaller pores should be established in the middle region of the sheet in an impulse dryer to help inhibit delamination.

Further experimental work compared a perforated and non-perforated membrane. It was found that the perforated membranes had higher values for critical pressure than

non-perforated membranes. It is believed that part of the reason for this increase in pressure is due to a geometric effect. Analysis was conducted to this end; while an increase in pressure was seen in the predicted pressures, it was unclear what other factors affect the increased critical pressure of the perforated membranes. However, these results suggest that larger pores near the heated roll and felt surfaces will help to vent steam from the middle region of the wet web. Therefore, lower levels of refinement in these regions should help inhibit delamination.

Further work, should extend to wet paper itself. Much work has been done by Lundh & Fellers [12] with regards to the energy release rate of dry paper. The amount of force necessary to pull a sheet apart was measured at a constant rate of extension; allowing the authors to establish the amount of work done on the paper. This allowed them to find the critical energy release rate in the out of plane direction for paper (Z-toughness). A similar technique should be applied to wet paper. Figure 6.1 shows a schematic of the concept. Figure 6.2 shows an actual set of jaws that wet paper can be set in and held with a vacuum.

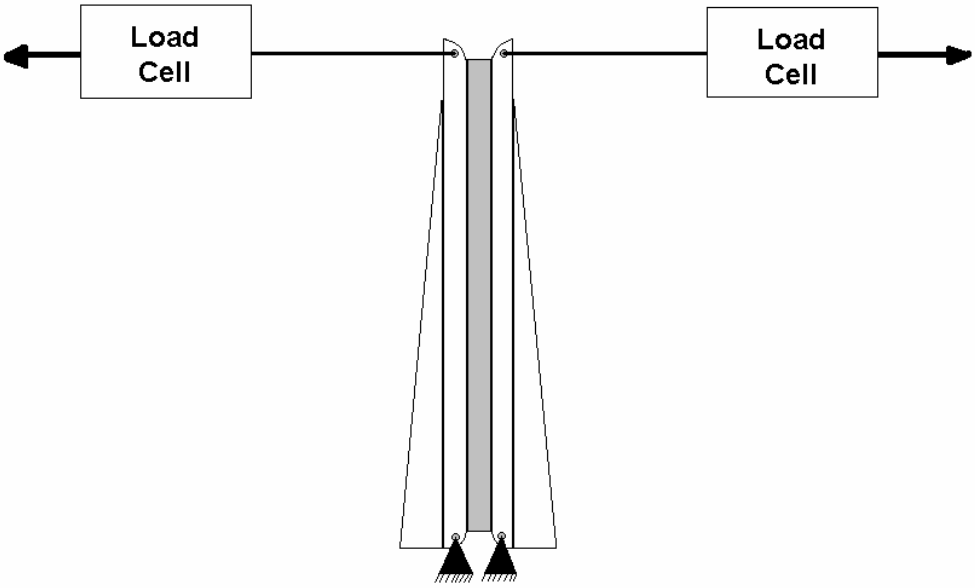

Figure 6.1: Schematic of Z-Toughness Apparatus for Wet Paper

Figure 6.2: Z-Toughness Jaws for Future Work

The jaws can be pulled at a constant rate of extension, while measuring the force. A horizontally oriented biaxial tester would be a suitable platform for such a test; it would be possible to set either a constant force or rate of extension, while measuring the other parameter. This would provide a solid method for measuring the critical energy release rate of wet paper. This data could be used in conjunction with level of refinement to estimate the pressure at which blisters and delamination would begin. This knowledge should be used to explore what variables in the furnish (i.e. additives, refinement, etc) affect the critical energy release rate and critical pressure of wet paper at various solids contents.

APPENDIX A

RAW DATA

A.1 Peel Tests

Table A-1: Results from Peel Tests of Latex and Epoxy

Test	Disp (m)	Load (N)	Stress (Pa)	Strain	G_a (N/m)	τ^c (N/m)
2a	0.015537	0.83586502	259638	0.2832	37.57	32.90807
2b	0.021151	0.83586502	259119	0.2826	37.56	32.90807
3a	0.018712	0.716474795	329537	0.3594	33.28	28.20767
3b	0.016594	0.955299727	406791	0.4437	45.95	37.61023
4a	0.0111	0.597040088	275059	0.3000	27.03	23.50552
4b	0.016575	0.597040088	227375	0.2480	26.42	23.50552
5b	0.014797	0.83586502	291801	0.3182	38.14	32.90807
6a	0.009292	1.074734434	336534	0.3670	50.08	42.31238
6b	0.009547	0.955299727	350881	0.3827	44.81	37.61023
7b	0.008447	0.716474795	370180	0.4037	33.90	28.20767
8a	0.00559	0.597040088	184152	0.2008	25.87	23.50552
8b	0.006858	0.597040088	204286	0.2228	26.12	23.50552
9a	0.034595	0.83586502	308475	0.3364	38.44	32.90807
9b	0.014485	0.597040088	258496	0.2819	26.82	23.50552
10a	0.022417	0.83586502	259119	0.2826	37.56	32.90807
10b	0.015226	0.83586502	370170	0.4037	39.55	32.90807
13a	0.005913	0.716474795	217753	0.2375	31.56	28.20767
13b	0.011631	0.597040088	210322	0.2294	26.20	23.50552
14a	0.005271	0.358215157	144217	0.1573	15.21	14.10296
14b	0.005482	0.597040088	289192	0.3154	27.21	23.50552
15a	0.008877	0.716474795	224351	0.2447	31.66	28.20767
15b	0.01236	0.955299727	344353	0.3756	44.67	37.61023
16a	0.01027	0.358215157	146115	0.1594	15.23	14.10296
16b	0.025272	0.83586502	396206	0.4321	40.02	32.90807

	G_a (N/m)	τ^c (N/m)
Average	33.37	28.79
St Dev	9.03	7.11

A.2 Critical Pressure Results

Table A-2: Pressure Experiment Results

Radius (m)	Tension (N/m)	Experimental Pressure (kPa)	τ^c λ_c (kPa)	Simple Griffith λ_c (kPa)	Griffith w/ Radial Strain λ_c (kPa)
0.0052063	62.12	13.08	12.93	25.09	10.56
0.0052975	62.98	10.78	12.66	24.82	10.38
0.0072831	58.71	8.27	9.41	17.43	7.55
0.0074609	63.41	8.79	8.97	17.69	7.37
0.0075373	63.41	6.20	8.88	17.51	7.29
0.0077786	62.98	9.26	8.62	16.91	7.07
0.0081694	62.12	8.79	8.24	15.99	6.73
0.0083247	58.28	6.07	8.25	15.20	6.60
0.009317	62.55	8.60	7.21	14.07	5.90
0.0093706	61.27	5.29	7.21	13.84	5.87
0.0093751	62.98	8.67	7.15	14.03	5.86
0.0097919	64.69	10.68	6.80	13.61	5.62
0.0101684	65.11	8.31	6.54	13.15	5.41
0.0101793	60.84	6.11	6.66	12.70	5.40
0.0101928	57.86	7.25	6.76	12.37	5.39
0.0111569	65.97	8.80	5.94	12.06	4.93
0.0117267	65.97	5.42	5.65	11.48	4.69
0.0124893	63.83	5.30	5.35	10.60	4.40
0.0148833	62.12	5.37	4.52	8.78	3.69
0.0150488	65.97	3.32	4.40	8.94	3.65
0.0152981	63.41	4.39	4.38	8.63	3.59
0.0157375	60.84	4.14	4.30	8.21	3.49

A.3 Perforation Tests

Table A-3: Raw Data for Black Tape Perforation Tests

Black Tape

Non-Perforated			Perforated		
Plate	**λ_c (kPa)**	**Average (kPa)**	**Plate**	**λ_c (kPa)**	**Average (kPa)**
A	22.06	23.44	A	48.26	48.26
	24.82			46.89	
B	18.62	18.62		49.64	
	19.31		B	42.75	43.21
	17.93			44.13	
C	16.55	15.86		42.75	
	15.17		C	27.58	30.57
	15.86			31.72	
D	9.65	10.34		32.41	
	9.65		D	23.44	22.75
	11.03			22.75	
	11.03			22.06	

Table A-4: Average Values for Black Tape

Black Tape Averages

Pore Radius (m)	λ_c (kPa)		
	Non-Perforated	Perforated	Geometric
0.003175	23.44	48.26	27.10
0.0047625	18.62	43.21	19.79
0.00635	15.86	30.57	16.41
0.009525	10.34	22.75	10.50

Table A-5: Raw Data for Clear Tape Perforation Tests

Clear Tape

Non-Perforated			Perforated		
Plate	**λ_c (kPa)**	**Average (kPa)**	**Plate**	**λ_c (kPa)**	**Average (kPa)**
	137.90	137.90		165.47	163.18
A	137.90		A	151.68	
	137.90			172.37	
	110.32	105.72		137.90	128.70
B	96.53		B	124.11	
	110.32			124.11	
	89.63	86.41		82.74	87.33
C	95.15		C	96.53	
	74.46			82.74	
	82.74	73.54		75.84	75.84
D	68.95		D	68.95	
	68.95			82.74	

Table A-6: Average Values for Clear Tape

Clear Tape Averages

Pore Radius (m)	λ_c (kPa)		
	Non-Perforated	Perforated	Geometric
0.003175	137.90	163.18	159.27
0.0047625	105.72	128.70	112.45
0.00635	86.41	87.33	89.43
0.009525	73.54	75.84	74.67

A.4 Iterative Solutions to Griffith Polynomial

Table A.7 gives the solutions for the critical pressure of equation (3.25). Sample calculations for the solution of this polynomial are given in Appendix B.3.

Table A-7: Solutions from EES for λ_c as a function of Defect Radius

Defect Radius (m)	λ_c (kPa)
0.0052	10.56
0.0053	10.38
0.0073	7.55
0.0075	7.37
0.0075	7.29
0.0078	7.07
0.0082	6.73
0.0083	6.60
0.0093	5.90
0.0094	5.87
0.0094	5.86
0.0098	5.62
0.0102	5.41
0.0102	5.40
0.0102	5.39
0.0112	4.93
0.0117	4.69
0.0125	4.40
0.0149	3.69
0.0150	3.65
0.0153	3.59
0.0157	3.49

APPENDIX B

SAMPLE CALCULATIONS

B.1 Critical Tension Sample Calculations

Critical Tension Model Example Calculation

$a = 0.205$ Pore Radius [in]

$\tau = 0.3547$ Tension in the Membrane [lb/in]

$\tau_c = 0.169$ Critical Tension , [lb/in]

$$K = \frac{2 \cdot \tau_c}{\sqrt{1 - \left[\frac{\tau_c}{\tau}\right]^2}}$$

$$\lambda_c = \frac{K}{a}$$

$\lambda_{c,SI} = \lambda_c \cdot 6.89476$

Solutions from EES yield\

a=0.205
K=0.3844
lambda_c=1.875
lambda_c_SI=12.93
tau=0.3547
tau_c=0.169

B.2 Simple Griffith Model Sample Calculations

Critical Tension Model Example Calculation

$a = 0.205$ Pore Radius [in]

$\tau = 0.3547$ Tension in the Membrane [lb/in]

$G_a = 0.196$ Critical Tension , [lb/in]

$$\lambda_c = \frac{2 \cdot \sqrt{2 \cdot \tau \cdot G_a}}{a}$$

$\lambda_{c,SI} = \lambda_c \cdot 6.89476$

Solutions From EES yield
a=0.205
G_a=0.196
λc=3.638
$\lambda_{c,SI}$=25.08
τ=0.3547

B.3 Griffith Model with Radial Strain Sample Calculations

$\nu = 0.24$ Poisson Ratio

$G_a = 0.196$ Critical Energy Release Rate, lb/in

The Coefficients of Bloom's Griffith Criterion Model that takes radial strain into account are given belc

$$A = \frac{1 + 2 \cdot \nu}{(1 + \nu)^2}$$

$$B = \frac{-(1 - \nu)}{2 \cdot E \cdot h}$$

$$C = \left[\frac{1 + 9 \cdot \nu}{16 \cdot (1 + \nu)}\right] \cdot \frac{(1 - \nu^2)^2}{E^2 \cdot h^2}$$

$$D = \frac{1 - \nu^2}{4 \cdot E \cdot h}$$

Bloom's Equation governing critical pressure, is solved by EES iteratively

$$G_a = \frac{E \cdot h}{2 \cdot (1 - \nu^2)} \cdot (A + B \cdot \lambda_c \cdot x + C \cdot \lambda_c^2 \cdot x^2) + D \cdot \lambda_c^2 \cdot x^2$$

The critical pressure is converted to SI units

$\lambda_{c,SI} = \lambda_c \cdot 6.89476$

Solutions from EES yield
A=0.9625
B=-2.034
C=4.051
D=1.261
E=50.96
G_a=0.196
h=0.003667
lambda_c=1.532
lambda_c_SI=10.56
nu=0.24
x=0.205

APPENDIX C

IMAGE ANALYSIS

C.1 Image Analysis

The goal of image analysis is to find the area and subsequently the radius of the initial defect. Primarily it was thought that this radius would be solely dependent on the size of the hole in the plate, however, it turned out to be nearly independent of that. The epoxy basically forms its own surface to which the latex adheres. So the epoxy forms the defect radius. This surface is not easily discerned by mechanical means, that is to say, it is difficult to use a ruler to estimate the initial defect radius of the non-circular defect. To find the size of the defect formed by the epoxy, a picture was taken and the area was found using a program called ImageJ.

The software is used for a variety of optical analysis functions throughout the scientific community. It has a built-in area function. The area function works on the concept of contrast. It looks at the pixels in a photograph, and assigns values to the intensity of different colors, based on the contrast of those values an area can be selected and the number of pixels within it can be counted. Knowing the size of the pixels, one can say what area of the selected item is.

The procedure then is to take a picture of the system, with some way some scale to judge the size of the pixels. Pictures from after the test are used, because the defect is filled with betadine, a very dark light absorbent material. This allows us to see the size of the initial defect better than before the test. Then the image is converted to a gray scale, this is necessary to use one of ImageJ's tools known as Threshhold; this allows one to differentiate where the contrasting areas are by using different filters. The area can then be selected and measured. The process is shown in more detail below.

Step 1: Picture with Scale

Figure C.1 shows the original photo, note how easily discernible the initial defect is, this is due to the high contrast between the betadine and the reflective stainless steel plate. At this point the scale is set using the c

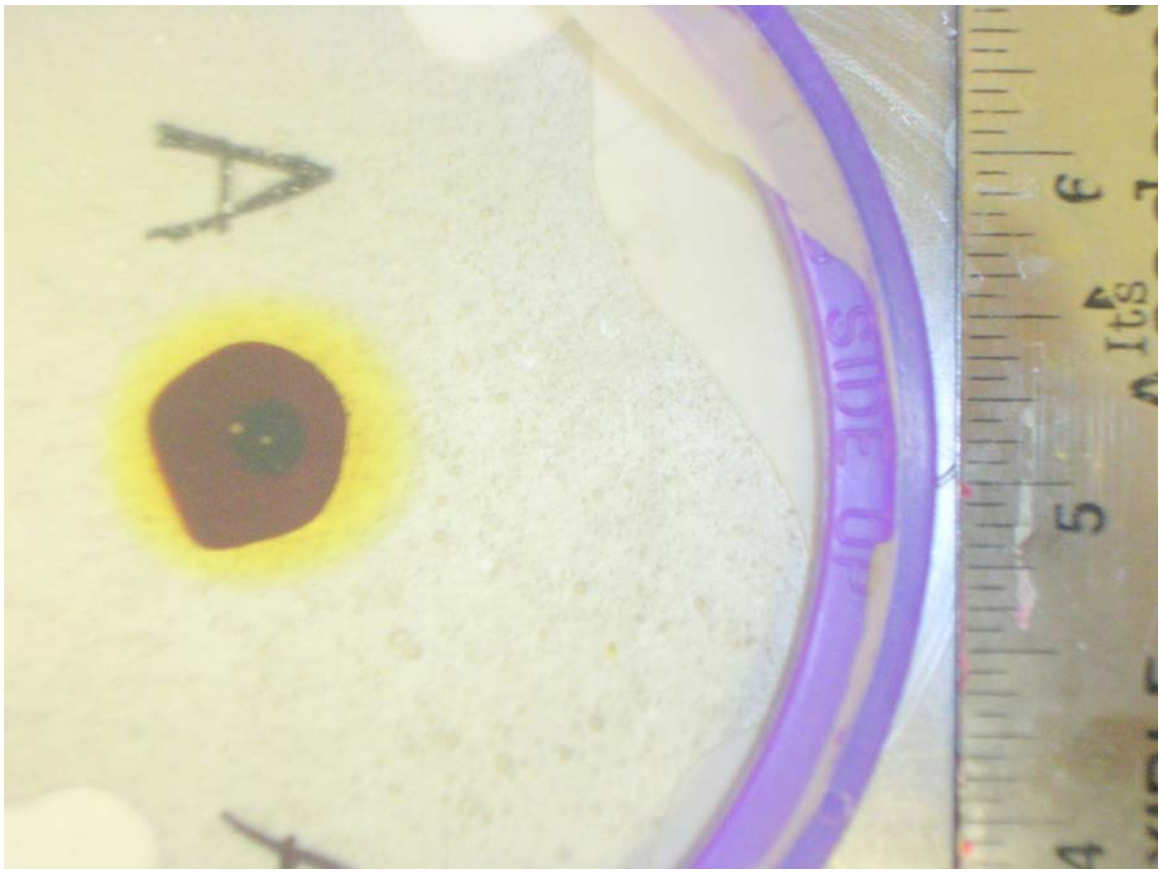

Figure C.1: Original Picture with Scale

Step 2: Set Scale

This is done by selecting the line tool, and marking a line along the ruler. Next select the following commands from the command bar, *Analyze>>Set Scale…* and set the

length of the line. This is shown in Figure C.2. Now convert the image to an 8-bit image to use the threshold tool; the commands are *Image>>Type>>8 bit.*

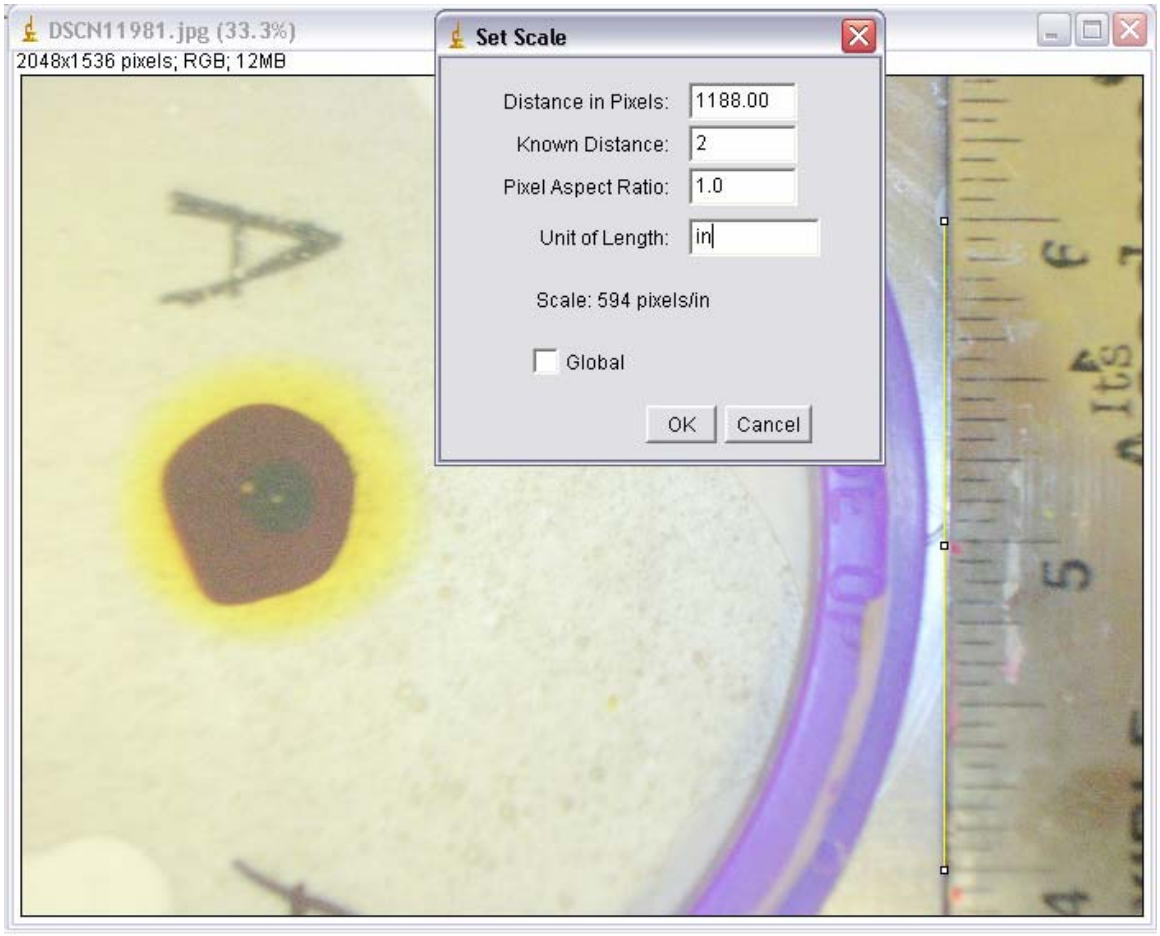

Figure C.2: Set the Scale

Step 3: Use threshold to select the area

Zoom in on the area using the zoom tool from the command bar and select the threshold tool, the commands are *Image>>Adjust>>Threshold*. This is shown in Figure C.3. The sliders of the threshold tool are adjusted back and forth until the edge of the defect is found. It takes some amount of trial and error to find the boundary of the defect, this is largely the reason why multiple images are taken and compared to establish the initial defect area and radius.

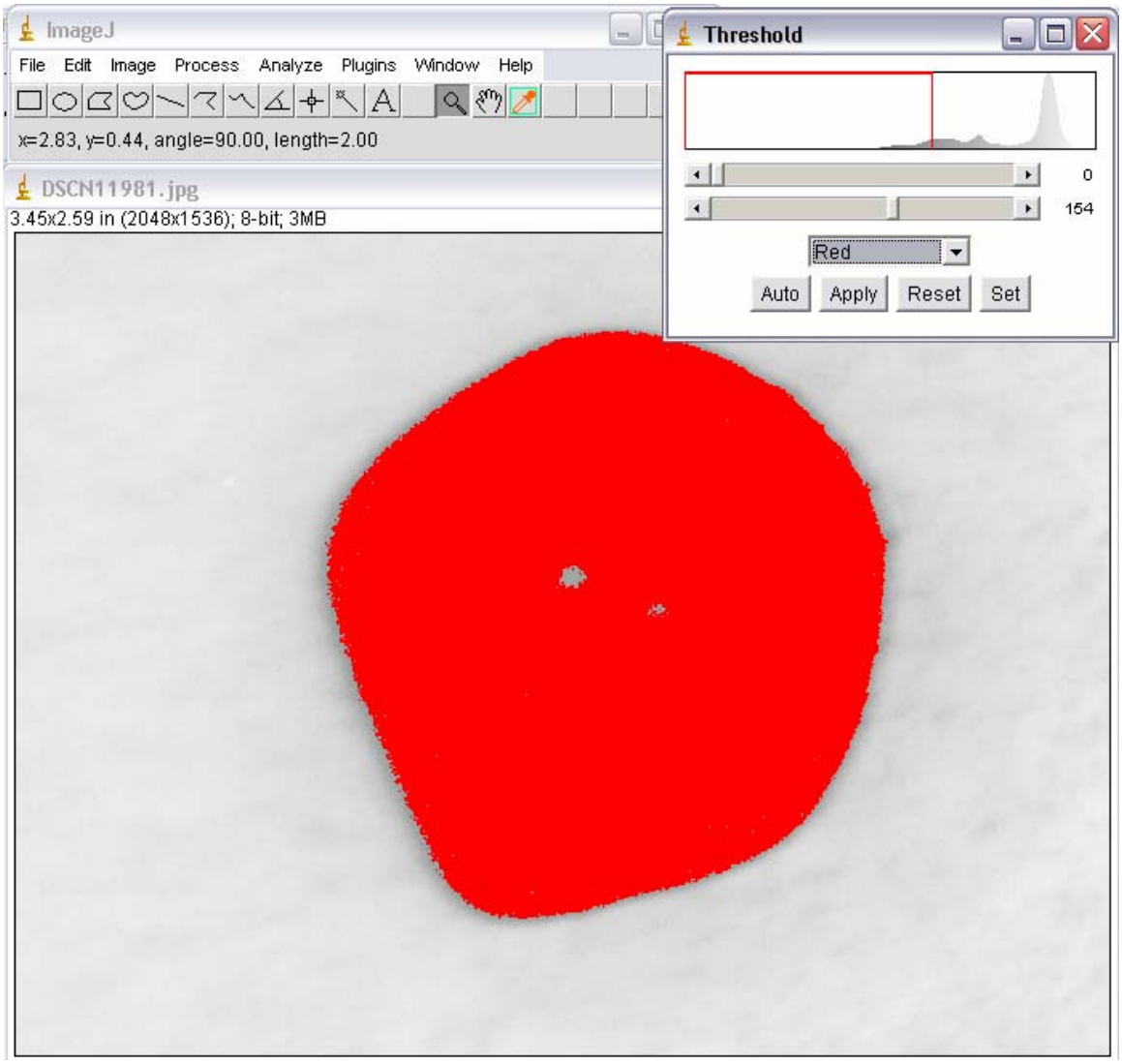

Figure C.3: Adjust Threshold

Step 4: Select the Area & Measure

Finally, the area of the defect can be measured. Select the contrasted area with the magic wand tool on the command bar. The command for the measure functions are *Image>>Measure.* Figure C.4, shows what this looks like, recall the area is in square

inches. The area of the defect is 0.2729 in^2, assuming a circular defect, the defect radius is 0.2947 in. Two more samples should be taken to ensure the validity of this number.

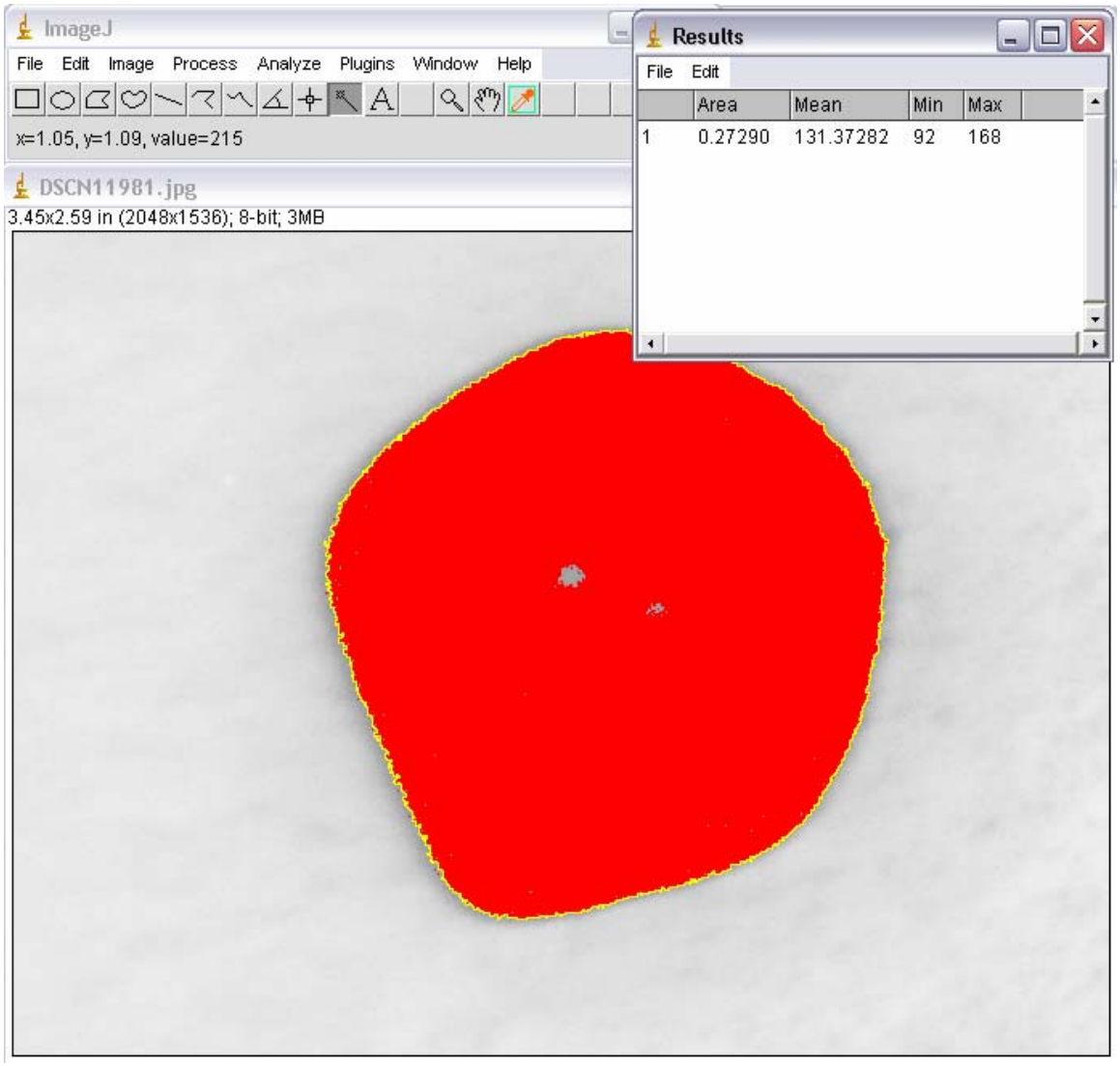

Figure C.4: Measure the Defect Area

APPENDIX D

MATH MODEL

D.1 Math Model

2 The Mathematical Model I. Quasi-Static Deflection

In this section we put forth a sequence of models whose purpose is to provide criteria for determining the critical pressure, λ_c, at which the membrane will separate from the plate; this critical pressure corresponds to that value of λ at which the glue bond, which holds the edge of the initially circular membrane fixed along the boundary of the hole in the plate, of radius a, will begin to fracture. Our first set of criteria all involve a quasi-static deflection.

2a Criterion No. 1

Our first criterion is based on the simple idea that in order to initiate fracture of the glue bond along the boundary of the membrane, at $r = a$, the component of the tensile force/length along the boundary normal to the plate must achieve a critical magnitude τ^c.

If (see fig. 1) we assume that under the action of a constant hydrostatic pressure λ all the equilibrium positions of the membrane are axially symmetric parabolids of revolution, then any slice perpendicular to the plate will yield a parabola of the form

$$w - w_M = \alpha r^2 \tag{2.1}$$

and, as $w(a) = 0$, $\alpha = -(w_M/a^2)$ so that

$$w(r) = w_M \left(1 - \left(\frac{r}{a}\right)^2\right) \tag{2.2}$$

where $w_M = w_M(\lambda)$ is the pressure dependent maximum deflection at $r = 0$. As w must satisfy the standard equation governing static deflection of a thin elastic membrane, e.g.,

$$\tau \left(w_{,rr} + \frac{1}{r} w_{,r}\right) = -\lambda \tag{2.3}$$

where τ is the constant magnitude of the tension in the membrane, and $w_{,r} = \dfrac{dw}{dr}$, $w_{,rr} = \dfrac{d^2w}{dr^2}$, substitution of (2.2) into (2.3) yields

$$w_M(\lambda) = \left(\frac{a^2}{4\tau}\right) \lambda \tag{2.4}$$

so that

$$w(r) = \frac{\lambda}{4\tau}(a^2 - r^2) \tag{2.5}$$

Remarks: The form of the deflection in (2.5) also follows, of course, directly from (2.3), which is equivalent to

$$r w_{,rr} + w_{,r} = -\frac{\lambda}{\tau} r$$

or

$$\frac{d}{dr}(rw_{,r}) = -\frac{\lambda}{\tau}r \tag{2.6}$$

Integration of (2.6) yields

$$w_{,r} = -\left(\frac{\lambda}{2\tau}\right)r + C_1 \tag{2.7}$$

If we impose the condition that $w_{,r}(0) = 0$, then $C_1 = 0$ and from (2.7) we obtain

$$w(r) = -\left(\frac{\lambda}{4\tau}\right)r^2 + C_2 \tag{2.8}$$

Finally, imposition of the boundary condition $w(a) = 0$ leads to

$$C_2 = \left(\frac{\lambda}{4\tau}\right)a^2$$

and, thus, once again to (2.5).

With reference to fig. 2, and in view of the fact that by (2.2)

$$\tan\phi = \left|\frac{dw}{dr}(a)\right| = \frac{2w_M}{a} \tag{2.9}$$

we infer that

$$\sin\phi = \frac{2w_M/a}{\sqrt{1 + (4w_M^2/a^2)}}$$

or

$$\sin\phi = \frac{2w_M}{\sqrt{a^2 + 4w_M^2}} \tag{2.10}$$

Therefore, for the magnitude of the component of the tension in the membrane, in the direction perpendicular to the plate, along the boundary at $r = a$, we have

$$|\tau_z| = \tau\sin\phi \equiv \frac{2\tau w_M}{\sqrt{a^2 + 4w_M^2}} \tag{2.11}$$

Thus, if $|\tau_z| = \tau^c$ then, as

$$w_M(\lambda_c) = \left(\frac{a^2}{4\tau}\right)\lambda_c \tag{2.12}$$

$$\tau^c = 2\tau\left(\frac{a^2}{4\tau}\right)\lambda_c \Big/ \sqrt{a^2 + \frac{a^4}{4\tau^2}\lambda_c^2}$$

which simplifies to

$$\tau^c = \frac{a\lambda_c}{2\sqrt{1+\frac{a^2\lambda_c^2}{4\tau^2}}} \tag{2.13}$$

Squaring both sides of (2.13) and solving for λ_c, the critical pressure, in terms of the critical z-direction tensile force/length along the boundary at $r = a$, we obtain

$$\lambda_c = \frac{2\tau^c}{a\sqrt{1-(\tau^c/\tau)^2}} \tag{2.14}$$

From (2.14) we deduce that the critical pressure varies inversely with the radius of the hole, i.e.,

$$\lambda_c = K(\tau;\ \tau^c)/a \tag{2.15}$$

The maximal deflection $w_M(\lambda_c)$ of the membrane at the point where delamination occurs is, by virtue of (2.12) and (2.14),

$$w_M(\lambda_c) = \left\{\frac{\tau^c/2\tau}{\sqrt{1-(\tau^c/\tau)^2}}\right\} a \tag{2.16}$$

while by (2.5) the deflected shape $w_c(r)$ of the membrane surface at criticality is

$$w_c(r) = \left(\frac{a}{8\tau}\right)\frac{\mu}{\sqrt{1-\mu^2}}\,(a^2-r^2) \tag{2.17}$$

where we have set $\mu = \tau^c/\tau$.

2b Criterion No. 2

Our second criterion is based on Griffith fracture mechanics and requires the computation of the net energy expended to deform the membrane, i.e.,

$$\Pi_a = -\frac{1}{2}\int\int_{R_a}\left\{\tau|\nabla w|^2 - 2\lambda w\right\} dA \tag{2.18}$$

where $R_a = \{(r,\theta)|0 \le r \le a,\ 0 \le \theta < 2\pi\}$ and

$$|\nabla w|^2 = w_{,x}^2 + w_{,y}^2 \equiv w_{,r}^2 \tag{2.19}$$

for a function - $w = w(r)$ of the radial coordinate only. In view of (2.5), $w_{,r} = -\lambda r/2\tau$, so

$$\Pi_a = -\frac{1}{2}\int\int_{R_a}\left\{\frac{\lambda^2}{4\tau}r^2 - \frac{\lambda^2}{2\tau}(a^2-r^2)\right\} dA \tag{2.20}$$

which is easily brought into the form

$$\Pi_a = -\frac{1}{2}\int_0^{2\pi}\int_0^a (\Gamma_1\lambda^2 r^2 - \Gamma_2\lambda^2 a^2) r\,dr\,d\theta \tag{2.21}$$

with

$$\Gamma_1 = \Gamma_1(\rho,\tau) \equiv \frac{3}{4\tau} \tag{2.22a}$$

$$\Gamma_2 = \Gamma_2(\rho,\tau) \equiv \frac{1}{2\tau} \tag{2.22b}$$

The interated integral in (2.21) is easily computed and yields

$$\Pi_a = \frac{\pi\lambda^2 a^4}{16\tau} \tag{2.23}$$

The membrane will delaminate provided the increase in energy per unit area of delamination exceeds the energy release rate $\mathcal{G}_a$. If delamination occurs, and the membrane radius increases by an amount Δa, then to terms of order $O((\Delta a)^2)$ the associated strain energy is given, in view of (2.23), by

$$\Pi_{a+\Delta a} = \frac{\pi\lambda^2}{16\tau}(a^4 + 4a^3\Delta a) \tag{2.24}$$

so that the change in strain-energy is

$$\Pi_{a+\Delta a} - \Pi_a = \frac{\pi\lambda^2}{4\tau}a^3\Delta a \tag{2.25}$$

The change in debonded area is $\Delta A = 2\pi a\Delta a$ so the change in energy per unit of debonded area will be

$$\lim_{\Delta a\to 0}\frac{\Pi_{a+\Delta a} - \Pi_a}{\Delta A} = \frac{\lambda^2}{8\tau}a^2 \tag{2.26}$$

Thus, the critical pressure for delamination λ_c is determined by equating the result in (2.26) to $\mathcal{G}_a$ in which case

$$\lambda_c = \frac{2\sqrt{2\tau\mathcal{G}_a}}{a} \tag{2.27}$$

Therefore, for fixed τ, $\lambda_c \sim a^{-1}$, which is in agreement with the prediction in (2.15). Using (2.27) we find that at delamination

$$w_M(\lambda_c) \equiv \left(\frac{a^2}{4\tau}\right)\lambda_c = \sqrt{\frac{\mathcal{G}_a}{2\tau}}a \tag{2.28}$$

Finally, in view of (2.2) and (2.28), the membrane configuration at the point of delamination, is given by

$$w_c(r) = \sqrt{\frac{G_a}{2\tau}}a\left(1-\left(\frac{r}{a}\right)^2\right) \tag{2.29}$$

2c Criterion No. 3

Our third criterion is also based on Griffith fracture mechanics but generalizes the membrane theory in that it takes into account radial strain. Our starting point is the coupled system of equations from plate theory for the displacement $w = w(r,t)$ and the stress function $\Phi = \Phi(r,t)$:

$$\rho\frac{\partial^2 w}{\partial t^2} - K\Delta^2 w = [\Phi, w_o + w] + \lambda \tag{2.30a}$$

$$\frac{1}{Eh}\Delta^2\Phi = -\frac{1}{2}[w,w] - [w_o, w] \tag{2.30b}$$

where the stiffness

$$K = \frac{Eh^3}{12(1-\nu^2)}$$

with E the Young's modulus and ν the Poisson ratio. Also

$$[w,\Phi] = w_{,rr}\left(\frac{1}{r}\Phi_{,r} + \frac{1}{r^2}\Phi_{,\theta\theta}\right) \tag{2.31}$$

$$+\left(\frac{1}{r}w_{,r} + \frac{1}{r^2}w_{,\theta\theta}\right)\Phi_{,rr}$$

$$-2\left(\frac{1}{r}w_{,r\theta} - \frac{1}{r^2}w_{,\theta}\right)\left(\frac{1}{r}\Phi_{,r\theta} - \frac{1}{r^2}\Phi_{,r}\right)$$

while

$$[w,w] = w_{,rr}\left(\frac{1}{r}w_{,r} + \frac{1}{r^2}w_{,\theta\theta}\right) - \left(\frac{1}{r}w_{,r\theta} - \frac{1}{r^2}w_{,\theta}\right)^2 \tag{2.32}$$

The form of the biharmonic operator Δ^2 will be specified below. If, as we shall assume, $K \simeq 0$, then the strain energy associated with bending is negligible and, thus, the net strain energy is given by the following expression, where u_r is the radial displacement:

$$U_a = \frac{\pi Eh}{1-\nu^2}\int_0^a \left\{\left(u_{r,r} + \frac{1}{2}w_{,r}\right)^2 + 2\nu\left(u_{r,r} + \frac{1}{2}w_{,r}^2\right)\frac{u_r}{r} + \left(\frac{u_r}{r}\right)^2\right\} r\,dr \tag{2.33}$$

while the potential energy is

$$V_a = 2\pi\lambda\int_0^a wr\,dr \tag{2.34}$$

and the total energy is $U_a + V_a \equiv \Pi_a$. The linearized strains for a thin membrane can be taken to be

$$\begin{cases} \varepsilon_{rr} = u_{r,r} \\ \varepsilon_{\theta\theta} = \dfrac{u_r}{r} + \dfrac{1}{r}u_{\theta,\theta} \\ \varepsilon_{r\theta} = u_{\theta,r} - \dfrac{u_\theta}{r} + \dfrac{1}{r}u_{r,\theta} \end{cases} \tag{2.35}$$

These strain components are further simplified if, as we shall assume, $u_\theta = 0$ and $u_{r,\theta} = 0$; in this case

$$\varepsilon_{rr} = u_{r,r};\ \varepsilon_{\theta\theta} = \frac{u_r}{r};\ \varepsilon_{r\theta} = 0 \tag{2.36}$$

The averaged stresses are given by

$$\begin{aligned} N_r &= \frac{Eh}{1-\nu^2}(\varepsilon_{rr} + \nu\varepsilon_{\theta\theta}) \\ N_\theta &= \frac{Eh}{1-\nu^2}(\varepsilon_{\theta\theta} + \nu\varepsilon_{rr}) \end{aligned} \tag{2.37}$$

while $N_{r\theta} = 2Gh\varepsilon_{r\theta} = 0$. In terms of the stress function $\Phi(r,t)$

$$N_r = \frac{1}{r}\Phi_{,r};\ N_\theta = \Phi_{,rr} \tag{2.38}$$

while $N_{r\theta} = \dfrac{1}{r}\Phi_{,\theta} - \dfrac{1}{r}\Phi_{,r\theta}$ vanishes.

As $w_{,\theta} = 0$ and $\Phi_{,\theta} = 0$, if $w_o = 0$, the static version of (2.30a,b) assumes the form

$$[\Phi, w] = -\lambda \tag{2.39a}$$

$$\Delta^2\Phi = -\frac{1}{2}Eh[w,w] \tag{2.39b}$$

where

$$[w,\Phi] = [\Phi,w] = \frac{1}{r}w_{,rr}\Phi_{,r} + \frac{1}{r}w_{,r}\Phi_{,rr} \tag{2.40a}$$

$$[w,w] = \frac{2}{r}w_{,r}w_{,rr} \tag{2.40b}$$

and

$$\Delta^2\Phi = \Phi_{,rrrr} + \frac{2}{r}\Phi_{,rrr} - \frac{1}{r^2}\Phi_{,rr} + \frac{1}{r^3}\Phi_{,r} \tag{2.41}$$

If we combine (2.36) with (2.37) we obtain the relations

$$\frac{1}{r}\Phi_{,r} = \frac{Eh}{1-\nu^2}\left(u_{r,r} + \nu\frac{u_r}{r}\right) \tag{2.42a}$$

$$\Phi_{,rr} = \frac{Eh}{1-\nu^2}\left(\frac{u_r}{r} + \nu u_{r,r}\right) \tag{2.42b}$$

From (2.39a), (2.40a), and (2.42a,b) it then follows that

$$\frac{Eh}{1-\nu^2}\left\{\left(u_{r,r} + \nu\frac{u_r}{r}\right)w_{,rr} + \left(\frac{u_r}{r} + \nu u_{r,r}\right)\frac{1}{r}w_{,r}\right\} = -\lambda \tag{2.43}$$

or, if we set

$$\begin{cases} a(r) = u_{r,r} + \nu\dfrac{u_r}{r} \\ b(r) = \dfrac{1}{r}\left(\dfrac{u_r}{r} + \nu u_{r,r}\right) \end{cases} \tag{2.44}$$

that

$$a(r)w_{,rr} + b(r)w_{,r} = \frac{-\lambda(1-\nu^2)}{Eh} \tag{2.45}$$

Remarks: Equation (2.45) may be compared with the standard membrane equation (2.3) for a function $w = w(r)$; the two equations, obviously, agree provided $a(r) = 1, b(r) = \frac{1}{r}$, and

$$\frac{1}{\tau} = \frac{1-\nu^2}{Eh} \tag{2.46}$$

The second of our equations, i.e., (2.39b), has the explicit form

$$\Phi_{,rrrr} + \frac{2}{r}\Phi_{,rrr} - \frac{1}{r^2}\Phi_{,rr} + \frac{1}{r^3}\Phi_{,r} = \frac{-Eh}{\tau}w_{,r}w_{,rr} \tag{2.47}$$

We observe that if Φ is quadratic in r, i.e., if $\Phi(r) = \alpha r^2 + \beta r + \gamma$ then, as $N_r = \frac{1}{r}\Phi_{,r}$ the condition that $N_r(0) < \infty$ implies that $\Phi_{,r}(0) = 0$ and, thus, that $\beta = 0$. Therefore, for a quadratic Φ,

$$\frac{1}{r}\Phi_{,r} = \Phi_{,rr} = 2\alpha$$

and, as a consequence of (2.42a,b), (2.43) reduces to

$$w_{,rr} + \frac{1}{r}w_{,r} = -\lambda/2\alpha \tag{2.48}$$

which is in agreement with (2.3) if we take $\alpha = \frac{\tau}{2}$. For a quadratic Φ of the form $\Phi(r) = \alpha r + \gamma$, however, $\Delta^2\Phi = 0$; this can be reconciled with (2.47), for small h, as follows: with

$\alpha = \tau/2$, (2.48) coincides with (2.3) so that $w(r)$ is given by (2.5). As a direct consequence of (2.5)

$$-\frac{Eh}{r}w_{,r}w_{,rr} = -\frac{Eh\lambda^2}{4r^2}$$

and, therefore, (2.47) is (approximately) satisfied for $\Phi(r) = \alpha r^2 + \gamma, \alpha = \tau/2$, provided

$$E\lambda^2 << \tau^2/h \tag{2.49}$$

As a further consequence of (2.42a,b), and the assumption that $\Phi(r) = \alpha r^2 + \gamma$, we have

$$u_{r,r} + \nu\frac{u_r}{r} = \frac{u_r}{r} + \nu u_{r,r} \tag{2.50}$$

so, for $\nu \neq 1$

$$u_{r,r} - \frac{1}{r}u_r = 0 \tag{2.51}$$

from which it easily follows that

$$u_r = Cr \tag{2.52}$$

However, in view of (2.42a) and the assumption that $\Phi(r) = \alpha r^2 + \tau$, with $\alpha = \tau/2$,

$$\frac{Eh}{1-\nu^2}\left(u_{r,r} + \nu\frac{u_r}{r}\right) = \tau \tag{2.53}$$

Employing (2.52) in (2.53) leads to the result that

$$C = \tau\left(\frac{1-\nu}{Eh}\right)$$

in which case we find as the (approximate) solution of (2.39a,b)

$$u_r = \tau\left(\frac{1-\nu}{Eh}\right)r \tag{2.54a}$$

$$w = \frac{\lambda}{4\tau}(a^2 - r^2) \tag{2.54b}$$

with $\tau = \dfrac{Eh}{1-\nu^2}$; therefore,

$$u_r = \left(\frac{1}{1+\nu}\right)r \tag{2.55a}$$

$$w = \frac{(1-\nu^2)\lambda}{4Eh}(a^2 - r^2) \tag{2.55b}$$

By virtue of (2.33), (2.34), the total energy Π_a has the explicit form

$$\Pi_a = \frac{\pi Eh}{1-\nu^2}\int_0^a \left\{\left(u_{r,r}+\frac{1}{2}w_{,r}\right)^2 + 2\nu\left(u_{r,r}+\frac{1}{2}w_{,r}^2\right)\frac{u_r}{r} + \left(\frac{u_r}{r}\right)^2\right\} r\,dr \\ +2\pi\lambda\int_0^a wr\,dr \tag{2.56}$$

Substituting (2.55a,b) into (2.56) yields

$$\Pi_a = \frac{\pi Eh}{1-\nu^2}\int_0^a \{A + B\lambda r + C\lambda^2 r^2\}\, r\,dr + 2\pi\lambda^2 D\int_o^a (a^2-r^2) r\,dr \tag{2.57}$$

where

$$\begin{cases} A = (1+2\nu)/(1+\nu)^2 \\ B = -(1-\nu)/2Eh \\ C = \dfrac{1+9\nu}{16(1+\nu)}\dfrac{(1-\nu^2)^2}{E^2h^2} \\ D = (1-\nu^2)/4Eh \end{cases} \tag{2.58}$$

The integrations in (2.57) produce the expression

$$\Pi_a = \frac{\pi Eh}{1-\nu^2}\left(\frac{1}{2}Aa^2 + \frac{1}{3}B\lambda a^3\right) + \frac{\pi}{4}\left(\frac{Eh}{1-\nu^2}C + 2D\right)\lambda^2 a^4 \tag{2.59}$$

We now proceed as in (2.24) and compute that, with an increase in membrane radius by an amount Δa,

$$\Pi_{a+\Delta a} = \frac{\pi Eh}{1-\nu^2}\left(\frac{1}{2}A[a^2+2a\Delta a] + \frac{1}{3}B\lambda[a^3+3a^2\Delta a]\right) \\ +\frac{\pi}{4}\left(\frac{Eh}{1-\nu^2}C + 2D\right)\lambda^2[a^4+4a^3\Delta a]$$

Therefore, up to terms of order $O((\Delta a)^2)$,

$$\Pi_{a+\Delta a} - \Pi_a = \frac{\pi Eh}{1-\nu^2}(Aa\Delta a + B\lambda a^2\Delta a) \\ +\pi\left(\frac{Eh}{1-\nu^2}C + 2D\right)\lambda^2 a^3\Delta a \tag{2.60}$$

in which case

$$\lim_{\Delta a\to 0}\frac{\Pi_{a+\Delta a}-\Pi_a}{\Delta A} = \frac{Eh}{2(1-\nu^2)}(A+B\lambda a) + \left(\frac{Eh}{2(1-\nu^2)}C + D\right)\lambda^2 a^2$$

and this leads to the following condition for delamination, namely,

$$\frac{Eh}{2(1-\nu^2)}\{A + B\lambda_c a + C\lambda_c^2 a^2\} + D\lambda_c^2 a^2 = \mathcal{G}_a \tag{2.61}$$

REFERENCES

[1] Bermond, C. "Establishing the Scientific Base for Energy Efficiency in Emerging Pressing and Drying Technologies." *Applied Thermal Engineering* 17.8-17.10 Aug.-Oct. 1997: 901-910.

[2] Mendes, Paula; Belgacem, Naceur; Bloch, Jean-Francis; Impulse Drying Technology: the state of the art and the recent advances; ATIP

[3] Krause, A M, Orloff, D I; Opening the Operating Window of Impulse Drying: I The Effect of Ambient Pressure at Nip Opening; 1997 TAPPI Engineering & Papermakers Conference

[4] Parviainen, P M, Orloff, D I; Opening the Operating Window of Impulse Drying: II. Pressure Differential as a Source of Delamination, 1997 TAPPI Engineering & Papermakers Conference

[5] Boerner, J, Orloff, D I; The Effect of Basis Weight and Freeness on Sheet Permeability and Critical Impulse Drying Temperature; TAPPI Engineering Conference, 1993

[6] Bloom, Fred; Orloff, David; Carter, Bart; On the Delamination of a Circular Membrane Under Hydrostatic Pressure, DATE?, JOURNAL?

[7] Dannenberg, H; Measurement of Adhesion by a Blister Method, Journal of Applied Polymer Science, v 5(1) pp 125-134, 1961

[8] Williams, M L, The Continuum Interpretation for Fracture and Adhesion, Journal of Applied Polymer Science, v 13 pp 29-40 1969

[9] Gent, A N, Lewandowski, L H; Blow-Off Pressures for Adhering Layers, Journal of Applied Polymer Science, v 33 pp 1567-1577, 1987

[10] Williams, J G, Energy Release rates for peeling of flexible membranes and the analysis of blister tests, Int Journal of Fracture v 87, pp265-288, 1997

[11] Hinkley, J A; A Blister Test for Adhesion of Polymer Films to SiO_2; J Adhesion v 16 pp 115-126, 1983

[12] Lundh, A, Fellers C; The Z-toughness method for measuring the delamination resistance of paper; Nordic Pulp and Paper Research Journal, v 16 (4) pp 298-305, 2001

[13] Arjun, A, Wan, K T; Derivation of the strain energy release rate G from first principles for the pressurized blister test; International Journal of Adhesion & Ahesives v 25 pp 13-18, 2005

[14] Mossakovskii, V I, Rybka, M T; Generalization of the Griffith-Sneddon Criterion for the Case of a Non-Homogeneous Body; PMM v 28 (6) pp 1061-1069, 1964

[15] Rice, J R, Sih, G C; Plane Problems of Crack in Dissimilar Media; Journal of Applied Mechanics, pp 418-423, 1965

[16] Carter, Barton P; Orloff, David I; Patterson, Tim; Development of Bulk in Printing and Writing Grades by Flash Evaporation; AMRC Mid-Year Report; Jan 2005